Published in final edited form as:
Physica A. 2015 January 15; 418: 126–153. doi:10.1016/j.physa.2014.07.045.

Biophysics of protein-DNA interactions and chromosome organization

John F. Marko
Department of Physics & Astronomy and Department of Molecular Biosciences, Northwestern University, Evanston, Illinois USA 60208

Abstract

The function of DNA in cells depends on its interactions with protein molecules, which recognize and act on base sequence patterns along the double helix. These notes aim to introduce basic polymer physics of DNA molecules, biophysics of protein-DNA interactions and their study in single-DNA experiments, and some aspects of large-scale chromosome structure. Mechanisms for control of chromosome topology will also be discussed.

Keywords

DNA; DNA-protein interactions; chromosome structure; chromosome dynamics

1. Introduction

DNA molecules in cells are found in double helix form, consisting of two long polymer chains wrapped around one another, with complementary chemical structures. The double helix encodes genetic information through the sequence of chemical groups - the “bases” adenine, thymine, guanine and cytosine (A,T,G and C). Corresponding bases on the two chains in a double helix bind one another according to the complementary base-pairing rules A=T and G≡C. These rules follow from the chemical structures of the bases, which permit two hydrogen bonds to form between A and T (indicated by =), versus three that form between G and C (indicated by ≡). Each base pair has a chemical weight of about 600 Daltons (Da).

The presence of the two complementary copies along the two polynucleotide chains in the double helix provides redundant storage of genetic information and also facilitates DNA replication, via the use of each chain as a template for assembly of a new complementary polynucleotide chain.

1.1. Basic physical properties of the DNA double helix

The structure of DNA gives rise to a number of interesting physical properties.

Stiffness—The DNA double helix is a moderately stiff semiflexible polymer, with a persistence length of about 50 nm (containing 150 base pairs or bp; there are approximately 0.34 nm per base pair along the double helix). The thickness of the double helix is about 2 nm, so a persistence length of double helix DNA is long and thin.

Length—Double-helix DNAs *in vivo* are generally very long polymers: the chromosome of the λ bacteriophage (a virus that infects *E. coli* bacteria) is 48502 bp or about 16 microns in length; the *E. coli* bacterial chromosome is 4.6×10^6 bp (4.6 Mb) or about 1.5 mm long; small *E. coli* "plasmid" DNA molecules used in genetic engineering are typically 2 kb to 10 kb (0.7 to 3 microns) in length; and the larger chromosomal DNAs in human cell nuclei are roughly 200 Mb or a few cm in length.

Electrical charge—The environment in the cell is essentially aqueous solution, in which DNA molecules are ionized, so as to carry essentially one electron charge per base (2 e^-/bp$\approx$ 6e^-/nm, each negative charge coming from an ionized phosphate on the DNA backbone, see Fig. 1(a)). The high electric charge density along the double helix makes it a strong polyelectrolyte, and gives it strong electrostatic interactions with other electrically charged molecules. Notably, in cells, the univalent salt concentration is 100 to 200 mM, making the Debye length shorter than 1 nm $\lambda_D \approx 0.3$ nm/ $\sqrt{M}$ where M is the concentration of 1:1 salt in mol/litre=M): thus electrostatic interactions with DNA, while strong, are essentially short-ranged. Electrostatic repulsions give rise to an effective hard-core diameter of dsDNA of $\approx$ 3.5 nm under physiological salt conditions [1].

Helical structure—The DNA double helix is really *two* polymers wrapped around one another, with one right-handed turn every $\approx$ 10.5 bp, or about 0.6 radian/bp (Fig. 1(b)). This, combined with the moderate strength of the base-pairing interactions holding the two strands together (about 2.5 k_BT per base pair when averaged over base-pair sequence) gives rise to the possibility of stress-driven structural defects ("bubbles" of locally base-unpaired single-strands) or transitions (stress-driven strand-separation). In addition, the two-strand structure implies the possibility of trapping a fixed linking number of the two strands when a DNA is closed into a loop. Constraint of strand linking number - a topological property of DNA - gives rise to a rich array of phenomena.

1.2. Proteins and DNA

DNA molecules by themselves are already quite interesting objects for biophysical study. However, the functions of DNA *in vivo* cannot be realized without the action of a huge number of *protein* molecules. Proteins are the workhorse molecules of the cell, and are themselves polymers of amino acids, folded into specific shapes by the action of relatively complex amino-acid-amino-acid interactions. Most proteins are in the range of 100 to 1000 amino acids in length (since amino acids are $\approx$ 100 Da on average, this corresponds to masses from 10^4 to 10^5 Da), and since each amino acid is about a cubic nanometer in volume, folded proteins are from a few to a few tens of nm in size.

DNAs in cells are covered with proteins, some of which interact rather specifically with short (< 20 bp) specific base-pair sequences, and some of which are less discriminating, interacting with DNA of essentially any sequence. Proteins that bind DNA tend to have positively charged patches on them to allow them to stick to the double helix (many DNA-binding proteins have a net positive charge in solution). Many proteins that bind DNA have hydrophobic amino acids which insert between bases, or hydrogen-bonding groups which link to corresponding hydrogen-bonding groups on the bases.

The functions of proteins which bind the double helix in cells are highly varied (Fig. 2). Some proteins bend the double helix so as to help it to be folded up to fit inside the cell (e.g., HU and Fis from *E. coli*, and histones from human and other eukaryote cells). Other proteins serve to mark specific sequences, providing platforms for more complicated activities of yet other proteins (e.g., *transcription factors* which trigger the copying of DNA sequence to RNA sequence, the primary step in the reading of a gene). Still other proteins catalyze cutting and resealing of the DNA backbone, allowing cut-and-paste and topological changes of DNA molecules to occur. More complex “protein machines” burn chemical fuels (including ATP, NTP, dNTP) to replicate, transcribe, and repair the double helix. Proteins thus give DNA its functions - its personality - in cells, turning a DNA molecule from just naked DNA, into a *chromosome*.

Many enzymes (proteins which perform catalytic functions) are used as tools to alter DNA structure in the test tube (“*in vitro*”): these include *restriction enzymes* which cut DNA at specific base-pair sequences; *DNA ligases* which reseal broken covalent backbones along DNA molecules; *topoisomerases* which change DNA topology. Combined with DNA base-pairing, which allows “hybridization” of different DNA molecules with complementary overhangs, these enzyme tools allow one to cut and paste different DNA segments together. Reinsertion of synthetic DNA segments into cells is the basis of genetic engineering. The same general methods allow DNA molecules to be end-attached to surfaces and particles in a selective, controlled manner, or to be assembled into human-designed nanoscale assemblies.

DNA-binding proteins generally distort and restructure the double helix (Fig. 2), making the mechanics of DNA important in thinking about its functions. The corollary is that DNA mechanics can be used to analyze protein-DNA interactions. This has been widely exploited in the past 15 years, via use of single-molecule DNA pulling and twisting experiments to study proteins acting along DNA. These notes are meant to provide some basic background in DNA statistical mechanics, some discussion of models useful for thinking about protein-DNA interactions from the point of view of single-DNA micromechanics experiments, and some description of biophysical problems associated with entire chromosomes.

1.3. Physical scales relevant to protein-DNA interactions

Length—The basic length scale relevant to molecular biology is the nanometer (nm= 10^{-9} m). DNA bases, amino acids, simple sugars, energy-transferring molecules such as ATP, and many of the other basic molecular units used by living things are all roughly 1 nm in size. Therefore, the nm is the scale of modularity of chemical structure, and also the scale of

information granularity. It is good to keep in mind that the length of a small bacterial cell or a small fraction of a eukaryote cell is $\approx 10^{-6}$ m or μm, 1000 nm in length.

Concentration—Another scale to remember is the concentration of one molecule per cubic micron, which is 10^{15} molecules per litre, or about 1.6×10^{-9} mol/litre= 1.6 nM (the number of molecules in a mol is $N_A \approx 6 \times 10^{23}$). This is very roughly the concentration of a transcription factor protein one might find in a bacterial or eukaryote cell.

Energy—There are two main energy scales of interest to us. First, there is the thermal energy per degree of freedom, $k_BT \approx 4 \times 10^{-21}$ J at room temperature (T = 300 K; for biological systems, T is never too far from this so we will regard k_BT as essentially fixed). The binding energies of the noncovalent bonds that hold biological molecules in their folded conformations (folded proteins, double helix structure of DNA) are naturally measured in k_BT units, e.g., base-pair binding energies along the DNA double helix range from ≈ 1 to $4k_BT$ per base pair under normal physiological solution conditions.

The second energy scale of relevance here is that of a covalent chemical bond, which is much larger, comparable to 1 eV $\approx 40k_BT$. This level of energy stabilizes the polymer backbones of protein and nucleic acid chains, and allows biological molecules to have their secondary (folded) structure changed, without breaking their primary (backbone) structure.

Force—The force scale most relevant to molecular biology is k_BT/nm$\approx 4 \times 10^{-12}$ N= 4 piconewtons (pN). The pN force scale appears as the characteristic force scale asssociated with biomolecule conformational change, since it corresponds to the breaking of noncovalent bonds of a few k_BT binding energy, by stretching them a fraction of a nm.

The few pN force scale should be contrasted with the much larger force scale of $\approx$eV/Å$\approx 10^{-9}$ N= 1 nN, the characteristic force one might expect to break a covalent bond [7].

We can quickly estimate the force scale to tear a protein off a DNA molecule (or to tear apart a dimeric protein complex). To do this one can expect to have to do a few k_BT of work over a reaction distance of a nm or so (the size of the binding site), indicating a rupture force of $\approx$ 10 pN in accord with experimental data, e.g., Ref. [8].

A lower force scale is associated with the force needed to prevent the initial looping of DNA by a protein that binds two sites ℓ apart. In this case, the work done against the applied force f is $\approx f\ell$ [9]. If looping is to occur by thermal fluctuation against that force, we can expect a strong suppression of the rate of loop formation relative to the zero-force case when $f\ell > 10k_BT$, or for $f > 10k_BT/\ell$ (for more detailed calculations including effects of DNA bending see Refs. [10, 11, 12]; note that DNA bending elastic energy controls loop formation rate at zero tension and is an *additional* free energy cost of loop formation, adding to the force-extension free energy).

For example, for ℓ = 100 nm (300 bp, a rather typical distance for loop formation by site-specific DNA-looping proteins as occurs during gene regulation) we have strong suppression of loop formation when $f > 0.1k_BT$/nm$\approx$ 0.4 pN. In this situation we expect the loop formation rate to be suppressed relative to the zero-force case by a factor $\approx e^{-10} <$

10^{-4}. Strong suppression of DNA looping by roughly piconewton forces has been observed [13, 14, 15].

A larger force is associated with the "stalling" of a molecular machine which burns ATP or similar energy-rich molecules, which transfer 10 k_BT into mechanical energy per step of nm dimensions. This stall force scale is roughly $\approx 10k_BT$/nm $\approx$ 40 pN. This is comparable to the stall forces observed for RNA and DNA polymerases [16, 17].

Time—At molecular scales, all dynamics is driven by thermal motion, and is highly overdamped: we don't need to worry about inertia for nm or even μm sized objects. All the motion we will worry about is diffusive, controlled by diffusion constants of the form $D = k_BT/(6\pi\eta R)$ where R is the scale size of the object in question (the formula is the Einstein diffusion constant for a sphere of radius R) and where η is the fluid viscosity ($\eta \approx 10^{-3}$ Pa·s for water, $\eta \approx 5 \times 10^{-3}$ Pa·s for cytoplasm). This gives rise to a self-diffusion time $\tau \approx 6\pi\eta R^3/(k_BT)$ which is on the order of 10^{-9} s for R = 1 nm, and about 1 s for R = 1 μm. The very strong R dependence of this diffusive relaxation time makes it change from a molecular timescale for nm-sized small molecules, to human-observable timescales for μm-scale objects.

2. The DNA double helix is a stiff polymer

The starting point for thinking about double helix DNA conformation is the semiflexible polymer, which models the double helix as having bending stiffness [18]. If we consider the double helix to have a fixed length L (not a bad approximation to start with), then we can describe it with a space curve $\mathbf{r}(s)$ where s is contour distance along the polymer, running from $s = 0$ to $s = L$. The tangent vector is a unit vector, $d\mathbf{r}/ds = \hat{\mathbf{t}}(s)$; the local curvature is $\kappa = |d\hat{\mathbf{t}}/ds|$. The polymer conformation is controlled by bending energy:

$$\beta E_{\text{bend}} = \frac{A}{2}\int_0^L ds \left(\frac{d\hat{\mathbf{t}}}{ds}\right)^2 \quad (1)$$

which is zero for the straight configuration $\kappa = 0$ ($\beta \equiv 1/[k_BT]$). The bending stiffness is controlled by the constant A, which has dimensions of length, and is called the *persistence length*. The flexible polymer limit is obtained for $L \gg A$; for $L \ll A$, the polymer will be essentially unbent by thermal fluctuations. For double helix DNA, $A \approx 50$ nm, or about 150 bp.

2.1. Statistical mechanics of the semiflexible polymer

Thermal fluctuations give rise to bending, and are described by the partition function

$$Z = \int \mathscr{D}\hat{\mathbf{t}}(s) \exp(-\beta E_{\text{bend}}) \quad (2)$$

where the notation $\mathscr{D}\hat{\mathbf{t}}$ indicates a path integral over $\hat{t}(s)$. This "free" polymer model (no applied force or self-interactions) can be solved in closed form [19]. The correlation function for the tangent vector is $\langle \hat{\mathbf{t}}(s) \cdot \hat{\mathbf{t}}(s') \rangle = e^{-|s-s'|/A}$. Since the end-to-end vector $\mathbf{R}$ can

be expressed in terms of the tangent vector via $\mathbf{R}=\mathbf{r}(L)-\mathbf{r}(0)=\int_0^L ds\hat{\mathbf{t}}(s)$, the mean square end-to-end distance can be computed from the tangent vector correlation function. This approaches the limit, for $L \gg A$, of $\langle R^2\rangle = \langle[\mathbf{r}(L) - \mathbf{r}(0)]^2\rangle = 2AL$, the scaling behavior for the coil size of a Gaussian polymer[1]. The correspondence between A and the statistical segment length b for the random flight or Gaussian polymers (for which $\langle R^2\rangle = Nb^2$) is $b = 2A$ and $N = L/(2A) = L/b$.

2.1.1. Stretching the semiflexible polymer by weak forces (< k_BT/A)—In the absence of force, since $\langle R^2\rangle = \langle x^2\rangle + \langle y^2\rangle + \langle z^2\rangle$ where x, y and z are the Cartesian components of the end-to-end vector $\mathbf{R}$, we have $\langle R^2\rangle = 3\langle x^2\rangle$. This zero-force fluctuation tells us the spring constant for linear response of a force applied to separate the ends, namely $k = k_BT/\langle x^2\rangle = 3k_BT/(2AL)$. This corresponds to the result for a Gaussian polymer, that the spring constant is inversely proportional to polymer length. The low-force response is $f = kx + o(x^3)$, with the linear response regime essentially holding for $f < k_BT/A$. For double helix DNA, this characteristic force is quite low since A = 50 nm; $k_BT/A \approx 0.1$ pN (recall $k_BT/(1$ nm$) \approx 4$ pN).

The linear low-force behavior is eventually replaced by the nonlinear scaling law for a self-avoiding polymer, for sufficiently large L [20]. However, for double-helix DNA, the narrow thickness ($\approx$ 3.5 nm including electrostatic effects[1]) of the double helix compared to its effective segment length $b = 2A \approx 100$ nm) leads to quite weak self-avoidance, and makes dsDNA elasticity quite close to that of an ideal polymer for DNA lengths (< 50 kb $\approx 16\ \mu$m) routinely studied experimentally [21].

2.1.2. Including external force in polymer models—For any polymer model, to go beyond linear force response, we need to include force in the energy function:

$$E = E_{\text{bend}} - \mathbf{f}\cdot\mathbf{R} \quad (3)$$

Force is added as a field conjugate to the end-to-end vector, so that expectation values of end-to-end extension appear as force derivatives of the partition function Z, as expected for identification of $k_BT \ln Z$ as a free energy in the fluctuating-extension, constant-force ensemble (the ensemble relevant to magnetic tweezers experiments, which apply a constant force to a paramagnetic particle attached to one end of a DNA [22]).

There are a number of general consequences for this form of statistical weight. For nonzero force along the z direction, or $\mathbf{f} = f\hat{\mathbf{z}}$, we have an average end-to-end extension $\langle z\rangle = \partial k_BT \ln Z/(\partial\beta f)$, and an extension fluctuation of $\langle z^2\rangle - \langle z\rangle^2 = \partial^2 \ln Z/\partial(\beta f)^2$. Components of $\mathbf{R}$ *transverse* to the force have zero average by symmetry ($\langle x\rangle = \langle y\rangle = 0$), but their fluctuations are nonzero, and are computed as $\langle x^2\rangle = \partial^2 \ln Z/\partial(\beta f_x)^2|_{\mathbf{f}=f\hat{\mathbf{z}}}$.

An important feature of any model of the form of Eq. (3) where there is no preferred orientation other than that of the force $\mathbf{f}$, is that the free energy only depends on the

[1]The general formula is $\langle R^2\rangle = 2AL\,[1 - (1 - e^{-L/A}\,A/L$ and has the small-L limit $\langle R^2\rangle = L^2$, see Ref. [19]

magnitude of force **f**, ln Z = ln $Z(|\mathbf{f}|)$. For nonzero force f along z, if we imagine applying small transverse forces f_x and f_z, we can expand $|\mathbf{f}|=\sqrt{f^2+f_x^2+f_y^2}=f+(f_x^2+f_y^2)/(2f)+\cdots$, and expand the partition function as

$$\ln Z(|\mathbf{f}|)=\ln Z(f)+\frac{f_x^2+f_y^2}{2f}\frac{\partial \ln Z(f)}{\partial f}+\cdots \quad (4)$$

A simple relationship between “longitudinal” and “transverse” derivatives of ln Z follows:

$$\frac{\partial^2 \mathrm{In} Z}{\partial(\beta f_x)^2}=\frac{1}{\beta f}\frac{\partial \ln Z}{\partial(\beta f)} \quad (5)$$

where both sides are evaluated for $f_x = f_y = 0$. This indicates that extension and transverse fluctuations are related: $\langle x^2\rangle = \langle z\rangle/(\beta f)$. Therefore, if we measure thermally averaged transverse fluctuations and average extension we can *infer* the applied force:

$$f=\frac{k_B T\langle z\rangle}{\langle x^2\rangle} \quad (6)$$

This *exact* relationship holds for *any* polymer model with a roationally symmetric conformational energy (essentially any model without a preferred direction in space other than the applied force, notably including models with polymer self-interactions) and is a powerful tool used for force calibration in magnetic tweezers experiments. Notably this relation is model-independent and not limited to the case of small fluctuations [12].

2.1.3. High-force behavior of the semiflexible polymer—We return to the specific case of the semiflexible polymer. Expressing the end-to-end vector $\mathbf{R}=\int_0^L ds\hat{\mathbf{t}}(s)$ allows us to rewrite the energy as a local function of $\hat{\mathbf{t}}(s)$, with force applied in the z direction (**f** = $f\hat{\mathbf{z}}$):

$$\beta E=\int_0^L ds\left[\frac{A}{2}\left(\frac{d\hat{\mathbf{t}}}{ds}\right)^2-\beta f\hat{\mathbf{z}}\cdot\hat{\mathbf{t}}\right] \quad (7)$$

In terms of $t(\hat{s})$, the energy is one-dimensional and local, which allows one to solve for the partition function using continuum transfer matrix (Schrodinger-like equation) methods [21].

The asymptotic high-force behavior is readily obtained using small-fluctuation analysis. We split the tangent vector into components longitudinal and transverse to applied force: $\hat{\mathbf{t}} = t_z\hat{\mathbf{z}} + \mathbf{u}$, with **u** in the *xy* plane. Since $|\hat{\mathbf{t}}|=1=\sqrt{t_z^2+u^2}$, we have $t_z = \hat{\mathbf{z}}\cdot\hat{\mathbf{t}} = 1 - u^2 + \cdots$. For large force, $\hat{\mathbf{t}}$ is aligned with $\hat{\mathbf{z}}$, so u is small; to Gaussian order we have

$$\beta E = -\beta f L + \frac{1}{2}\int_0^L ds\left[A\left(\frac{d\hat{\mathbf{u}}}{ds}\right)^2 + \beta f u^2 + \mathcal{O}(u^4)\right] \quad (8)$$

In terms of Fourier components ($\mathbf{u}_q \equiv \int_0^L ds e^{-iqs}\mathbf{u}(s)$, for $q = 2\pi m/L$, $n = 0, \pm 1, \pm 2, \cdots$) we have

$$\beta E = -\beta f L + \frac{1}{2L}\sum_q (Aq^2 + \beta f)|\mathbf{u}_q|^2 + \mathcal{O}(u^4) \quad (9)$$

Using the equipartition theorem,

$$\langle |\mathbf{u}_q|^2 \rangle = \frac{2L}{Aq^2 + \beta f} \quad (10)$$

where the factor of 2 in the numerator reflects the two (x and y) components of **u**. The form of this wavenumber-space correlation function indicates that the real-space bending correlations decay exponentially, $\langle u_i(s)u_j(s')\rangle \propto \delta_{ij}e^{-|s-s'|/\xi}$, with a high-force correlation length $\xi = \sqrt{k_B T A/f}$.

Fourier transforming[2] Eq. (10) gives the fluctuation of **u**,

$$\langle |\mathbf{u}(s)|^2 \rangle = 2\int_{-\infty}^{+\infty}\frac{dq}{2\pi}\frac{1}{Aq^2 + \beta f} = \frac{1}{\sqrt{\beta A f}} \quad (11)$$

This allows us to compute the average extension

$$\frac{\langle z \rangle}{L} = \langle \hat{\mathbf{z}} \cdot \hat{\mathbf{t}} \rangle = 1 - \frac{1}{2}\langle u^2 \rangle + \mathcal{O}(u^4) = 1 - \sqrt{\frac{k_B T}{4Af}} + \ldots \quad (12)$$

This characteristic reciprocal square-root dependence of extension on force for a semiflexible polymer in the regime $f \gg k_B T/A$ is observed in single-molecule experiments on double-helix DNA for forces from about 0.1 up to 10 pN (Fig. 3) [21].

2.2. Denaturation of DNA by stress

From thermal DNA "melting" (strand separation) studies, we know that the cohesive free energy holding the two single-stranded DNAs (ssDNAs) into double helix form is about $g = 2.5k_BT$ per base pair [23].[3] For forces in the ≈ 10 pN range, we can expect deformation of the secondary structure of any biological molecule which is stabilized by weak non-covalent

[2]The result shown is the long-polymer limit $L \to \infty$, where $\Sigma_q \to L \int dq/(2\pi)$

[3]$\approx 1k_B T$ for AT-rich sequences, and $\approx 4k_B T$ for GC-rich sequences, under "physiological" conditions of 150 mM univalent salt, pH 7.5, and room temperature

chemical bonds of binding energy $\approx k_BT$. This has been experimentally observed for double-helix DNA in a few different ways.

Unzipping—If one imagines grabbing the two ssDNAs at one end of a double helix and then forcing them apart, one can imagine "unzipping" of the two strands to occur. This has been done in a number of laboratories, with the result that the resulting ssDNA liberates about $\ell = 1$ nm per base pair "unzipped" (this length is shorter than twice the ≈ 1 nm length of the extended ssDNA length per base because of thermal fluctuations). Therefore the work done per base pair as the helix is unzipped should be $\Delta W \approx f\ell$. Since this work is done directly against the cohesive energy of the double helix, we could expect an unzipping force of $f_{\text{unzip}} \approx g/\ell \approx 2.5k_BT/\text{nm} \approx 10$ pN. This is in fact the approximate force observed for DNA unzipping, which is observed to range from 8 to 15 pN depending on sequence (essentially AT/GC content) [25, 26, 27, 28, 29, 30]. The *variations* in unzipping force have been proposed to be used to analyze DNA sequence.

Overstretching—If a large force is applied to the two opposite ends of a long dsDNA, one might expect lengthening of the double helix. In this geometry, the length increase is bound to be less since it is in the direction of the double helix (rather than perpendicular to it as for DNA unzipping). In such experiments, the double helix length per base pair increases from 0.34 nm/bp to about 0.6 nm/bp; again using the DNA strand separation free energy as the free energy scale, we obtain an overstretching forces of $f_{\text{overstretch}} \approx 2.5k_BT/(0.2\text{ nm}) \approx 50$ pN. In fact such an "overstretching" transition is observed at a well-defined force ≈ 65 pN [31, 32, 33].

Unwinding—One might also imagine a torque acting to unwind the DNA double helix, which would liberate a wrapping angle of about 0.6 rad/bp unwound (2π radians per 10.5 bp). The torque required for this should be, following the same arguments as above, $\tau_{\text{unwind}} \approx -2.5k_BT/(0.6\text{ rad}) \approx -4k_BT \approx -16$ pN·nm (the sign reflects the left-handed nature of the unwinding torque. Unwinding actually occurs for torques ≈ -10 pN·nm [34, 35, 36, 29, 37, 38]. (a slightly lower torque than the above estimate occurs since left-handed wrapping is driven after denaturation by a left-handed torque).

Experimental observations and more detailed theoretical work has resulted in development of a force-torque "phase diagram" for the double helix, with a variety of different structural states [36, 38, 39].

3. DNA-protein interactions

In cells, proteins cover the DNA double helix, allowing it to be stored, read, repaired, and replicated. Different proteins have different functions on the double helix:

Architectural: Proteins that help to package DNA, bending and folding it, typically binding to 10 to 20 bp regions and often without a great deal of sequence dependence; examples include histones (eukaryotes) and HU, H-NS and Fis (*E. coli*);

Regulatory: Proteins that bind to specific DNA sequences from 4 to 20 bp in length, and which act as "landmarks" for starting transcription or other genetic processes; examples include TATA-binding protein (eukaryotes) and Lac repressor (*E. coli*);

Catalytic: Proteins which cut and paste DNA, accomplishing breaking and resealing of the covalent bonds along the DNA backbone, or inside the bases; examples include topoisomerases, DNA oxoguanine glycosylase (Ogg1, an enzyme that recognizes and repairs oxidative chemical damage to the base guanine);

DNA-sequence-processing: Proteins which burn NTPs or dNTPs and which move *processively* along the DNA backbone, reading, replicating, unwinding or otherwise performing functions while translocating along DNA; examples include RNA polymerases, DNA polymerase and DNA helicases.

3.1. Classical two-state kinetic/thermodynamic model of protein binding a DNA site

The starting point for thinking about protein-DNA interactions is binary chemical reaction kinetics ($P + D \leftrightarrow C$) where P is a particular protein, D is one of its binding sites, and C is the protein-DNA bound "complex". Consider just one binding site in a sea of proteins at concentration c. Supposing diffusion-limited binding kinetics, we have to wait for a particular protein to "find" the binding site; the on-rate in this case is the result of Smoluchowski, $r_{on} = 4\pi Dac$ where D is the diffusion constant for the protein, and a is the "reaction radius", the distance between reactants at which the reaction occurs, a scale comparable in size to the binding site. Since $D \approx k_B T/(6\pi\eta R)$, where R is the approximate size of the protein, we have $r_{on} = k_{on}c$, where the chemical forward rate constant for the reaction is $k_{on} \approx (a/R)k_B T/\eta$. Since $R > a$ we can take $k_B T/\eta$ as a kind of "speed limit" for a binary reaction controlled by three-dimensional diffusion. For $T = 300$ K and $\eta = 10^{-3}$ Pa·s (appropriate for water at room temperature),

$$k_{on} < \frac{k_B T}{\eta} = \frac{4 \times 10^{-21}\mathrm{J}}{10^{-3}\mathrm{Pa \cdot s}} = 4 \times 10^{-18}\mathrm{m^3/s} \approx 10^{9}\mathrm{M^{-1}s^{-1}} \quad (13)$$

where the final units indicate a a rate per unit concentration (M = mol/litre; recall 1 M= 6×10^{23}/litre).

It turns out that this rate can be *increased* by roughly an order of magnitude if in addition to three-dimensional diffusion, there is also one-dimensional "search" over a restricted region of a long DNA polymer in which a specific binding site is embedded [40, 41]. However, the rate at which initial encounters of protein and DNA occur is still controlled by Eq. (13). There remain many interesting problems having to do with (small) proteins binding to a (long) DNA polymer, for example the dependence of multiple sequential interactions on polymer conformation [42].

Returning to the basic picture of proteins binding to one DNA binding site, once the complex is formed, one usually considers it to have a lifetime, described by a concentration-dependent rate k_{off} of dissociation of the protein from the DNA (units of k_{off} measured in s^{-1}).

Once our proteins come to equilibrium with the binding site, the probability that the site will be bound relative to being unbound will be

$$\frac{P_{\rm on}}{P_{\rm off}}=\frac{k_{\rm on}c}{k_{\rm off}}\equiv\frac{c}{K_d} \quad (14)$$

where the *dissociation constant* $K_{\rm D}\equiv k_{\rm off}/k_{\rm on}$ describes the strength of the binding. Since K_D is the concentration at which the site is 50% bound, the smaller K_D is, the tighter the binding.[4] The site-occupation probability is the familiar Langmuir adsorption isotherm, $P_{\rm on} = c/(K_D + c)$.

The Boltzmann distribution gives the equilibrium free energy difference between the bound and unbound states,

$$G_{\rm on}-G_{\rm off}=-k_BT\ln\frac{P_{\rm on}}{P_{\rm off}}=k_BT(\ln K_d-\ln c) \quad (15)$$

The bound state is reduced in free energy (becomes more probable) as solution concentration of protein is increased. Eq. (15) can be thought of as reflecting the free energy associated with interactions ($G_{\rm int} = k_BT \ln K_D$; smaller K_D gives a more negative "binding" free energy) in competition with the ideal gas entropy loss associated with localizing the protein to the DNA binding site ($G_{\rm ent} = -k_BT \ln c$; an ideal-gas entropy model is appropriate since the volume fraction of any particular DNA-binding protein species is usually very small *in vivo* or in test-tube experiments). This basic type of model is widely used to analyze protein-DNA interactions.

3.2. Salt-concentration-dependence of proteins binding to DNA

Although the two-state model described above is very useful, under many circumstances it is important to keep in mind even one protein binding a DNA is an interaction between macromolecules which are covered with adsorbed water molecules and ions. Even one binding interaction involves changing the positions of many molecules. In general proteins which bind to DNA make an array of non-covalent bonds to the double helix, and usually a number of those are electrostatic in character (say $n \approx 5$ to 10); the highly negatively charged phosphates along the DNA backbone are often found in registry with positively charged chemical groups along a bound protein. However, when the protein is dissociated, those same positive (protein) and negative (DNA) interaction sites have associated with them essentially "condensed" counterions. Thus binding of one protein to DNA results in *release* of 2*n* counterions. The resulting free energy of the released counterions gives rise to a dependence of the "interaction energy" on solution univalent ion concentration:

$$G_{\rm int}=k_BT\ln K_D+2nk_BT\ln(c_{\rm salt}/c_0) \quad (16)$$

[4] K_D is used widely by biochemists; note that the *equilibrium constant* used widely by chemists is just $K_{\rm eq}\equiv 1/K_D$

where K_D is the dissociation constant at salt concentration c_0. Since n is in the range of 5 to 10 for typical DNA-binding proteins, one can expect a strong dependence of binding free energy (affinity) on bulk salt concentration (lower salt: stronger binding; higher salt: weaker binding).

This behavior has been carefully studied for short basic polypeptides interacting with nucleic acid oligomers [43], but there is plenty of room for more studies of this type on "real" proteins interacting with DNA. There is a similar competition that can occur between a group of proteins binding small adjacent binding sites, and one large protein which binds all of their binding sites, a situation which arises in gene expression in eukaryotes [44].

3.3. Cooperativity

Biochemical cooperativity refers to the synergistic effect associated with two binding events which happen at once. The simplest example of this is the presence of a contact interaction between two proteins which bind adjacent binding sites along a DNA; if that contact interaction is favorable (lowering the net free energy), it is termed *cooperative*; if unfavorable, it is called *anticooperative*. If we imagine describing occupation of two adjacent binding sites using occupation variables n_1 and n_2 ($n_i = 0$ or 1 for empty or bound sites, respectively), then the general energy function describing the interactions of protein and DNA is

$$G_{\rm int} = G_1 n_1 + G_2 n_2 + G_c n_1 n_2 \quad (17)$$

For the four possible states, we have three interaction parameters (the unbound state $n_1 = n_2 = 0$ is taken as a reference state of zero free energy). If $G_c < 0$, we have a model of cooperative binding.

The analogy of Eq. (17) with Ising interaction between two spins in a field is useful, and generalization of this type of model to a string of interacting proteins can be used to describe "polymerization" of proteins along DNA, driven by adjacent-protein interactions [45, 46]. A variety of proteins have been observed to be able to form filaments along DNA. A classic example is RecA, which forms a helical filament as it binds along DNA [47]. RecA polymerization along DNA is thought to play a role in its function in searching along DNAs for regions of similar sequence or *homology*; the RecA filament is thought to act as both a scaffold and as a machine to test for sequence similarity along two juxtaposed DNA strands.

3.4. Force effect on protein-DNA binding

If tension f is present in a DNA molecule during interaction with proteins, that tension can affect the binding. In general there will be some mechanical change in length of the DNA if the protein binds; suppose there is a length contraction ℓ (or lengthening if $\ell < 0$) of the DNA molecule when binding occurs. As examples, imagine a protein which bends or loops DNA, cases for which $\ell > 0$. Tension plausibly slows down $k_{\rm on}$ (since now one must get to a transition state by doing work against the applied tension) and plausibly speeds up $k_{\rm off}$ (the chemical bonds in the complex will be destabilized by any applied tension). By Eq. (14), in

equilibrium, the ratio of these rates and therefore the binding/unbinding probability ratio reflect the presence of the additional mechanical work $f\ell$ [9]:

$$\frac{P_{\rm on}}{P_{\rm off}} = \frac{c}{K_D} e^{-\beta f \ell} \quad (18)$$

where $\beta = (k_B T)^{-1}$, and where K_D indicates the dissociation constant at zero force. Eq. (18) suggests that we identify a force-dependent dissociation constant, $K_D(f) = K_D(0) \exp(\beta f \ell)$ and for $\ell > 0$ we see that applied force increases the K_D strongly, since tension is destabilizing the bound complex.

This effect becomes dramatic for DNA looping. Note that even in the absence of force, the stiffness of the double helix essentially constrains thermally-formed loops to be longer than $\approx$ 50 nm (somewhat shorter loops can form but at a large free energy cost, *i.e.*, slowly). If tension is present, there is an additional force-retraction free energy cost [9]. For example, even a rather small loop with $\ell \approx 100$ nm under moderate tension of $f = 0.5$ pN will have $f\ell \approx 12.5 k_B T$, leading to a large perturbation of the K_D. In such a case, the on-rate will be most strongly affected (suppressed) by applied force, since the "transition state" for the looping reaction requires nearly all of the work $f\ell$ to be done by thermal fluctuation, if the protein-mediated looping interaction is of short range [10, 11].

3.5. A model for DNA-bending proteins binding along a long double helix

DNA in most organisms is covered with "architectural" DNA-bending proteins, to help package it compactly. In eukaryotes the "histone" proteins (two each of histones H2A, H2B, H3 and H4) complex together as octamers to form "nucleosomes", with each histone acting to bend DNA [48]. In addition a variety of small DNA-bending proteins act to further kink DNA between nucleosomes (including HMG proteins such as HMGB1). In bacteria, "nucleoid" proteins (in *E. coli*, Fis, HU, H-NS and StpA) act independently to generate bends along DNA [49]. These bacterial proteins will bind well to most DNA sequences, although they certainly all have affinities that vary with DNA sequence.

It is of interest to consider the situation where one has a long dsDNA subject to insertion of kinks when proteins bind to it; this situation has been studied in a variety of single-DNA experiments [50, 51, 52, 53, 54] and is a simplified version of the situation occurring *in vivo*. A simple polymer model that is useful for considering this situation is a discretized semiflexible chain model, where each segment is a potential binding site for a protein, which when present induces a bend [55]:

$$\beta E = \sum_{i=1}^{M} \left[\frac{a}{2} (\hat{\mathbf{t}}_{i+1} - \hat{\mathbf{t}}_i)^2 \delta_{n_i,0} + \frac{a'}{2} (\hat{\mathbf{t}}_{i+1} \cdot \hat{\mathbf{t}}_i - \cos\psi)^2 \delta_{n_i,1} - \beta f \ell \hat{\mathbf{z}} \cdot \hat{\mathbf{t}}_i - \beta \mu n_i \right] \quad (19)$$

This model divides a DNA molecule up into M segments of length ℓ, so the total length of the DNA is $L = M\ell$. At each segment there is a orientation variable $\hat{\mathbf{t}}_i$, and a protein occupation variable n_i which takes on values 0 and 1 for no protein or protein bound, respectively.

The orientations are principally controlled by applied force f. Protein binding is controlled by the chemical potential μ, and for ideal solution (suitable for describing the sub-micromolar protein concentrations used in most experiments) we can use the relation $\mu = k_B T \ln c + \varepsilon$, taking into account the ideal solution entropy loss and the binding energy gain associated with protein binding. When there are no proteins bound ($n_i = 0$) the bending stiffness of the chain is a, which is related to the continuum model persistence length via $A = a\ell$ in the continuum limit $\ell \to 0$. For double-stranded DNA, this model is reasonable since a protein binding site size is a few nm in length; using $\ell < 5$ nm defines a model with $\ell \ll$ A, and therefore with semiflexible polymer elasticity.

In this model, when a protein is bound to a segment, its local bending stiffness is modified (the a' term) and a kink is generated with preferred bending angle ψ. This couples the bending and binding degrees of freedom and makes the binding isotherm force-dependent. For the partition function $Z = [\prod_i \int d^2 t_i \Sigma n_i] \exp(-\beta E)$ we have the simple expectation value relations

$$\langle z \rangle \equiv \left\langle \sum_{i=1}^{M} \hat{\mathbf{z}} \cdot b\hat{\mathbf{t}}_i \right\rangle = \frac{\partial \ln Z}{\partial \beta f} \quad \langle P \rangle = \left\langle \sum_{i=1}^{M} n_i \right\rangle = \frac{\partial \ln Z}{\partial \beta \mu} \qquad (20)$$

where $\langle z \rangle$ and $\langle P \rangle$ are the end-to-end extension in the force direction and the total number of proteins bound, respectively. This type of model can be numerically solved using transfer matrix methods [55, 56], and one sees a shift of the force-extension curve to larger forces as protein concentration is increased (Fig. 4), as observed in corresponding experiments [50, 51, 52, 53, 57].

An interesting feature of this type of model (in particular any model where force is coupled to extension and where the binding chemical potential is coupled to occupation) is the "Maxwell relation" arising from the second mixed derivatives of the partition function [58]:

$$\left(\frac{\partial \langle z \rangle}{\partial \mu} \right)_f = \left(\frac{\partial \langle P \rangle}{\partial f} \right)_\mu \qquad (21)$$

This exact relation is potentially useful since it allows one to estimate changes in binding occupation $\langle P \rangle$ from measurements of force-extension curves:

$$\langle P \rangle_{f,\mu} = \langle P \rangle_{f_0,\mu} + \int_{f_0}^{f} df' \left(\frac{\partial \langle z \rangle}{\partial \mu} \right)_{f'} \qquad (22)$$

Interestingly, this purely thermodynamical relation is able to count changes in absolute numbers of molecules bound to a DNA. This type of model-free relation has been used to estimate protein binding changes with force [59, 57], torque changes in twisted molecules [60] (as proposed in Ref. [58]), and changes in ions bound to stretched nucleic acids[61].

An interesting feature of this type of model is the emergence of interactions, or cooperativity, between nearby proteins along the DNA without any *intrinsic* interactions

(*e.g.*, as in Eq. (17)) [56]. These interactions appear for nonzero force, because of the bends. If two nearby bends are oriented oppositely to one another, then they can compensate for one another, in the sense that the DNA can extend a little more [62]. The result is an *attractive* interaction between two DNA-bending proteins bound along a DNA, that can be quite strong for forces where the DNA is stretched out (the regime $f > k_BT/A$) [56]. For large forces the interaction effective energy has an exponential dependence on distance between the proteins $\propto e^{-|i-j|\ell/\lambda}$. One might expect this since in this regime the free energy of the DNA is determined by small-amplitude bending fluctuations with correlation length $\xi = \sqrt{k_BTA/f}$ (Eq. (10)). A surprise is that $\lambda = \xi/2$, half of what a naive argument based on Eq. (10) predicts. This factor of two difference arises due to rotational symmetry around the force axis [63]. This is an example of a situation where one has a local degree of freedom (the occupation number for protein occupation n_i) whose correlation function decays with a correlation length differing from that controlling the free energy (*i.e.*, distinct from the correlation length arising from the two largest eigenvalues of the transfer matrix).

Recently, it has been observed that there is another type of cooperativity acting between two nearby DNA-interacting proteins. A protein bound at one specific binding site has been observed to alter the binding properties of a second nearby (up to 15 bp away) binding site, with a DNA helical orientation dependent interaction. This effect is thought to be due to the "allosteric" deformation response of the DNA between the two proteins [64]. A reasonable model for this effect can be based on introduction of an interaction between nearby tangent vectors which introduces correlations in nearby bending angles (*i.e.*, in Eq. (19), correlations in $\hat{\mathbf{t}}_i \cdot \hat{\mathbf{t}}_{i+1}$) in a double-helix-orientation dependent fashion [65].

3.6. Concentration-dependent dissociation

In Sec. 3.1 we discussed the classical picture of the kinetics of protein binding and unbinding, where there is concentration-dependent binding ($r_{on} = k_{on}c$) and concentration-*independent* unbinding ($r_{off} = k_{off}$, just a constant rate). The concentration-independent off-rate model is generally assumed to describe biomolecule interactions, including protein-DNA binding. Note that this simple model assumes only two states: an "off", dissociated state, and an "on", bound state, with single transitions linking them (recall $P + D \leftrightarrow C$ from Sec. 3.1).

There is starting to be a fair amount of experimental evidence that this simple type of model with a constant off-rate is often inappropriate; a number of groups have reported solution-concentration-dependent off rates [66, 67, 68, 69, 70], *i.e.*, $k_{off}(c) = k_{off,0} + k_{off,1}c + \cdots$. In this kind of power-series expansion of the concentration-dependence of $k_{off}(c)$, the first term $k_{off,0}$ is the classical concentration-independent "decay" rate, or rate at which thermal fluctuations break the bonds holding the protein to the double helix. The second term $k_{off,\,1}$ introduces a linear dependence of the off-rate on concentration, and describes the interaction of one protein *in solution* with a bound protein. If $k_{off,\,1} > 0$, the protein in solution *increases* the rate at which the bound protein leaves the DNA.

This is possible if the protein in solution, the protein bound to the DNA, and the DNA itself form a *ternary* complex, *i.e.*, if both proteins simultaneously interact with the DNA. This

can happen at a single binding site, since a protein is not held on DNA by just one chemical bond, but instead is bound by an array of chemical interactions. One can imagine *partial* dissociation of a bound protein which allows a protein in solution to interact with part of its binding site. This second protein could plausibly *block* complete rebinding of the first protein, allowing it to dissociate and to be replaced by the second protein. The result of this would be an *exchange* of the first and second protein, at a rate of $k_{\mathrm{off},1}c$.[5]

One can write down a simple chemical reaction diagram for this (Fig. 5) based on a *two-step* dissociation pathway for a "two-bond" binding site. Many proteins that bind DNA have a dimeric structure, with two well-defined DNA-binding domains, see *e.g.*, Fig. 2 A-B, also see Ref. [71]; the two 'bonds' can be thought of as the binding of two DNA-binding domains to the two halves of a binding site. We suppose that an initially bound protein can be fully bound (state 1, held on by two bonds) or partially bound (state 1*, held on by only one bond). In the partially bound state, a second protein can *also* be partially bound (state 1*2*). In this new state, protein 1 is blocked from being fully bound by partial occupation of the binding site by protein 2, and has an appreciable probability of completely dissociating. If protein 1 dissociates, we are left with only protein 2 partially bound (state 2*), which we can take to be a state equivalent to state 1*. Solving the equilibrium for this model we can obtain the rate at which exchanges occur (the rate of transitions from 1*2* to 2*), which is concentration-dependent. For the model sketched in Fig. 5 the number of proteins that occupy the binding site is

$$n_{\mathrm{bound}}=\frac{2k_{12}^{'}(k_1+k_1^{'})k_0c+2k_1^{'}k_0k_2c^2}{k_1k_{1*}^{'}k_{12}^{'}+2k_{12}^{'}(k_1+k_1^{'})k_0c+k_1^{'}k_0k_2c^2} \quad (23)$$

The binding isotherm ceases to have the 'hyperbolic' form of the classical Langmuir-like model ($n_{\mathrm{bound}} = c/[K_D + c]$). If $k_{1*}^{'}$ is sufficiently slow compared to k_2c, exchange will dominate as the pathway to dissociation of an initially bound protein. Note that at high solution concentration, the binding saturates at *two* proteins per binding site. Simulations and more detailed calculations have provided additional information about this exchange-facilitated dissociation mechanism and have been used to quantitatively model experimental data[71, 72].

4. DNA topology

Topology of polymers generally refers to *linking* or *entanglement* properties, which are invariant under smooth geometrical deformations, and which can only change when one polymer passes through another. A simple example is the linking of two rings; they can be unlinked, or linked together; one cannot pass from the unlinked to a linked state without breaking one of the rings (Fig. 6).

[5]The units of $k_{\mathrm{off},1}$ are the same as k_{on}, *i.e.*, events per concentration per time, or $\mathrm{M}^{-1}\mathrm{s}^{-1}$.

4.1. Linking number

We can compute the *linking number* of two oriented closed curves by just counting up all of their mutual signed crossings, according to the rules shown in Fig. 7. Dividing the total crossing number by two gives an integer, the linking number Lk of the two curves (Fig. 6). This quantity can only change when one curve is passed through another. [6]

The Gauss invariant computes the same quantity, but determines it from the geometry of the two curves without directly counting their crossings:

$$\mathrm{Lk}=\frac{1}{4\pi}\oint_{C_1}\oint_{C_2}\frac{d\mathbf{r}_1\times d\mathbf{r}_2\cdot(\mathbf{r}_1-\mathbf{r}_2)}{|\mathbf{r}_1-\mathbf{r}_2|^3} \quad (24)$$

For DNA, we can distinguish between *external* linking of two double helix molecules together, and the *internal* linking property of the double helix itself.

4.1.1. Internal double-helix linking number LK—We first consider the *internal* linking of the two strands inside one double helix. The double helix contains two single-stranded DNAs which are wrapped around one another in a right-handed fashion, with a preferred twist rate of one turn every $n_h \approx 10.5$ bp, or every $h \approx 3.6$ nm of contour length. For helical wrapping, we can associate a linking number, which is just the number of times one strand crosses over the other [7]. For a double helix of length L and N_{bp} base pairs, $\mathrm{Lk} \approx \mathrm{Lk}_0 = L/h = N_{\mathrm{bp}}/n_h$. However, Lk is an integer for a closed double helix, and is not in general equal to Lk_0.

The difference between double helix linking number and the preferred linking number, $\Delta\mathrm{Lk} = \mathrm{Lk} - \mathrm{Lk}_0$, is often expressed as a fraction of the preferred linking number (linking number density), $\sigma \equiv \Delta\mathrm{Lk}/\mathrm{Lk}_0$ (the excess linking number per DNA length is $\Delta\mathrm{Lk}/L = \sigma/h$). In *E. coli* and many other species of bacteria, circular DNA molecules are maintained in a state of appreciably perturbed Lk, with $\sigma \approx -0.05$.

4.1.2. DNA twist stiffness—If Lk is sufficiently different from Lk_0, then there will be a buildup of twist in the DNA, leading to a geometrical response. This response is often a wrapping of the double helix around itself, a phenomenon known as *supercoiling*. One can observe this by taking a stiff cord and twisting it. This behavior arises from a competition between the bending energy (Eq. (1)) and the elastic twist energy,

[6]Linking topology is perfectly well defined only for closed curves or polymers. However, it is sometimes useful to define linkage of open curves, using suitably defined closure boundary conditions, *e.g.*, closing chains at infinity by extending them with long straight paths. This introduces small corrections to the properties of entanglement of interest here (primarily estimates of linking number). Qualitatively this can be understood by considering the definition of linking number in terms of signed crossings (Fig. 7). If we imagine deforming part of one of the links of Fig. 6 so that it closes far from the other crossings (not introducing any new crossings in the process) the topology and linking number of the polymer will be unchanged. This will be true for all closure paths that do not introduce additional strand crossings, indicating a rather weak dependence of linking number on closure boundary conditions, and further allowing us to talk about the topology of the region of the polymers *not including* the closure in a reasonably well-defined way. This is particularly true for linking of stretched polymers as will be discussed below; see, e.g., Ref. [73].

[7]For internal DNA linking the Gauss invariant is computed using orientation of the two backbones *in the same direction* along the double helix, giving positive crossings to right-handed wrapping.

$$\beta E_{\text{twist}} = \frac{C}{2L}\Theta^2 \quad (25)$$

where Θ is the net twist angle along the double helix. In the absence of other constraints, thermal fluctuations of twist give rise to a fluctuation

$$\langle \Theta^2 \rangle = \frac{L}{C} \quad (26)$$

suggesting the interpretation of the elastic constant C as a characteristic length for twist fluctuations. For the double helix, this *twist persistence length* is $C \approx 100$ nm. Note that the derivative of E_{twist} with respect to Θ is the torque or "torsional stress" in the DNA:

$$\tau = \frac{\partial E_{\text{twist}}}{\partial \Theta} = \frac{k_B T C}{L}\Theta \quad (27)$$

If there is no bending, then any excess linking number ΔLk goes entirely into twisting the double helix: $\Theta = 2\pi\Delta\text{Lk}$ (or $\sigma = \Theta/[2\pi L/h]$). The mechanical torque in DNA will be $\tau = 2\pi k_B T C \Delta\text{Lk}/L = (2\pi k_B T C/h)\sigma$. The parameter $2\pi C/h \approx 175$ sets the scale for when the linking number density will start to appreciably perturb DNA conformation, *i.e.*, when $|\tau| \approx k_B T$. This level of torque occurs for $|\sigma| \approx 0.005$.

4.1.3. Linking number LK, twist Tw and writhe Wr—The previous computation supposed that there was no bending, in which case all of the ΔLk is put into twisting the double helix. This DNA twisting can be quantified through the twist angle Θ, or equivalently through the twisting number [8].

If DNA bending occurs, there may be *nonlocal* crossings of the double helix over itself. These nonlocal crossings contribute to double helix linking number, and the separation of length scales between DNA thickness and the longer scale of DNA self crossing (controlled by the persistence length A) allows linking number to be decomposed into local (twist) and nonlocal (writhe) crossing contributions:

$$\text{Lk} = \text{Tw} + \text{Wr} \quad (28)$$

or equivalently, ΔLk = ΔTw + Wr.

One can demonstrate this with a thin strip of paper (30 cm by 1 cm works well). Put one twist into the strip, closing it in a ring. The two edges of the strip are linked together once. Now without opening the ring, let it assume a figure-8 shape; you will see that you can make the twist go away: in this state there is only writhe (Fig. 8)

[8]The total twist of a DNA molecule can be written as the excess twist ΔTw plus the intrinsic twist, or $\text{Tw} = \Delta\text{Tw} + \text{Lk}_0 = \Delta\text{Tw} + L/h$, where $\Delta\text{Tw} = \Theta/(2\pi)$.

For elastic ribbon models of DNA, suitable definition of the twist allows Wr to be expressed by the analytical formula [74, 75]:

$$\mathrm{Wr}=\frac{1}{4\pi}\oint_C\oint_C \frac{d\mathbf{r}_1\times d\mathbf{r}_2\cdot(\mathbf{r}_1-\mathbf{r}_2)}{|\mathbf{r}_1-\mathbf{r}_2|^3} \quad (29)$$

where $\mathbf{r}_1$ and $\mathbf{r}_2$ are the two edges of the ribbon. The similarity of this equation to the Gauss invariant, Eq. (24), arises from the partitioning of the double integral into contributions from local wrapping of the strands in the double helix (Tw), and from nonlocal contributions (Wr) arising from nonlocal crossings of the centerline of the molecule. Eq. (29) is the sum of the signed nonlocal crossings for *one* curve (following the rule of Fig. 7), averaged over all orientations [75]. A key point is that while Lk is a topological property, Wr and Tw are geometrical, and change value as the molecule is distorted.

4.1.4. DNA Supercoiling—The ability to transfer Tw to Wr suggests that when there is appreciable torsional stress in a flexible filament, it can be relaxed by wrapping the filament around itself. For DNA we should also include the entropic cost of bringing the filament close to itself. A type of model model widely used to describe the “plectonemic” wrapping of DNA around itself (Fig. 9) is based on treating the wrapping as helical, and by writing down a variational free energy [76, 77, 78, 39]:

$$\beta F=\frac{C}{2L}\Theta^2+\frac{AL}{2}\kappa^2+\frac{L}{(Ar^2)^{1/3}}+Lv(r) \quad (30)$$

where $\Theta = 2\pi\Delta Tw$ is the DNA twisting (which costs twist elastic energy), κ is the bending curvature, which is $\kappa = r/[r^2 + p^2]$ for a regular helix of radius r and pitch p (the intercrossing distance is $\ell = \pi p$, Fig. 9). The final two terms describe the entropic confinement free energy for a semiflexible polymer in a tube [79, 77, 80] and direct electrostatic and hard-core interactions per molecule length, $v(r)$.

The confinement entropy is based on estimation of the correlation length for bending fluctuations for a confined chain, which will have curvature fluctuations $\approx r/\xi^2$. The fluctuations in the bending free energy per length (in k_BT units) will be $\approx Ar^2/\xi^4$, and over a correlation length the fluctuation free energy is therefore $\approx Ar^2/\xi^3$. But the fluctuation free energy over a correlation length in k_BT units should be ≈ 1, giving us $\xi^3 \approx Ar^2$, and the confinement free energy per length (still k_BT units) of $\approx 1/\xi = 1/(Ar^2)^{1/3}$.

The important final ingredient is Eq. (28) which allows the twist to be expressed in terms of linking number and the writhe: $\Theta = 2\pi\Delta\mathrm{Tw} = 2\pi(\Delta\mathrm{Lk} - \mathrm{Wr})$. For a plectoneme based on regular helices, $\mathrm{Wr} = \mp Lp/(2\pi[r^2 + p^2])$ where the upper/lower signs are for right/left handed plectonemic wrapping [77].

Putting this together gives the free energy per length

$$\frac{\beta F}{L}=2\pi^2 C\left(\frac{\Delta \mathrm{Lk}}{L}-\frac{p}{2\pi(r^2+p^2)}\right)^2+\frac{A}{2}\frac{r^2}{(r^2+p^2)^2}+\frac{1}{(Ar^2)^{1/3}}+v(r) \quad (31)$$

where the sign of the writhe has been chosen to provide the lower twist energy for positive ΔLk, which is the case of a left-handed superhelix (note that left-handed plectonemes form for ΔLk > 0 while right-handed ones form for ΔLk < 0).

The free energy (31) can be optimized numerically to determine r and p [77, 81, 78, 39]. However, it is instructive to consider an approximate computation for the case of a slender superhelix ($r \ll p$), for which the curvature is $\kappa \approx r/p^2$, and the writhe per length is $\mathrm{Wr}/L \approx 1/(2\pi p)$, corresponding to one crossing per length 2ℓ of DNA. Dropping the molecular interaction potential $v(r)$ gives

$$\frac{\beta F}{L}\approx 2\pi^2 C\left(\frac{\Delta \mathrm{Lk}}{L}-\frac{1}{2\pi p}\right)^2+\frac{A}{2}\frac{r^2}{p^4}+\frac{1}{(Ar^2)^{1/3}} \quad (32)$$

Now, this expression can be minimized to determine optimal values of r and p. Up to numerical constants, minimization over r sets $Ar^2 \propto p^3$ (setting the correlation length for bending fluctuations in the plectoneme to $\xi \approx p$), and reduces the final two terms of Eq. (32) to k/p where k is a $O(1)$ constant. Subsequent minimization with respect to $1/p$ gives $-2\pi^2 C(\Delta \mathrm{Lk}/L - 1/[2\pi p]) + k = 0$, or $1/(2\pi p) = \Delta \mathrm{Lk}/L - k/(2\pi^2 C)$. There is a threshold $\Delta \mathrm{Lk}^* = k/(2\pi^2 C)$ for appearance of a valid minimum ($p > 0$), introduced by the entropic cost of confinement; in terms of superhelix density $\sigma = \Delta \mathrm{Lk}/(L/h)$ this is $\sigma^* = k/(2\pi^2 C/h)$, which is small compared to unity due to the ratio of length scales $C/h \approx$ (100 nm)/(3.6 nm). Beyond this characteristic value of linking number, the plectoneme becomes stable, and has a free energy below the essentially unwrithed, twisted molecule. This provides a rough idea of the behavior of the full plectoneme model Eq. (31) [76, 77, 81, 39]. For sufficient ΔLk, "screening" of the twist energy Eq. (25) by the writhe becomes favorable, which has little bending free energy cost if the superhelix radius r is kept relatively small.

Given that the main result for the free energy of the plectoneme is a free energy that rises from zero and eventually becomes superlinear, a useful approximate form to use for the free energy per length of the plectoneme is $\beta F(\sigma)/L = (2\pi^2 C_p/h^2)\sigma^2$, where $C_p \approx 25$ nm, $C_p < C$ reflecting the twist-energy-screening effect [82].

4.1.5. Twisting stretched DNA—In single-molecule DNA stretching experiments, if a force in the pN range is applied the double helix will be nearly straight. If it is then *twisted* while under ≈ pN forces, the molecule will tend to coil chirally, leading to a slight contraction. For small twisting, a small-fluctuation-amplitude computation can be done [83, 84], expanding the tangent vector fluctuations around the force direction (again $\mathbf{t} = t_z\hat{\mathbf{z}}+\mathbf{u}$, where $\mathbf{u}$ are the components of $\mathbf{t}$ perpendicular to $\hat{\mathbf{z}}$). We begin with the energy for a DNA under tension *and* twist:

$$\beta E=\frac{2\pi^2 C}{L}(\Delta\mathrm{Lk}-\mathrm{Wr})^2-\beta f L+\frac{1}{2}\int_0^L ds\left[\frac{A}{2}\left(\frac{d\mathbf{u}}{ds}\right)^2+\frac{\beta f}{2}\mathbf{u}^2\right]+\mathcal{O}(u^4) \quad (33)$$

just Eq. (8) with the addition of the twist energy. For a single-DNA experiment, ΔLk is just the number of full turns made of the end of the molecule (in a magnetic tweezers experiment, the number of times the magnet and therefore the bead at the end of the DNA is rotated [85]).

The challenge is how to include the linking number constraint in Eq. (33). The solution is to use an alternative representation of the writhe which takes the form of a *single integral* over contour length *s* [86]:

$$\mathrm{Wr}|_{\mathrm{mod}\ 1}=\frac{1}{2\pi}\oint\frac{\hat{\mathbf{z}}\cdot\hat{\mathbf{t}}\times d\hat{\mathbf{t}}}{1+\hat{\mathbf{z}}\cdot\hat{\mathbf{t}}} \quad (34)$$

The appearance of the “mod 1” in Eq. (34) reflects the fact that this expression for Wr (unlike the double integral Eq. (29)) is not sensitive to *antipodal points*, essentially nonlocal crossings which contribute ±1 to the total writhe (for a detailed discussion see Ref. [87]). The huge advantage of Eq. (34) over Eq. (29) is the presence of only a single integral, permitting expansion in powers of **u** for small deformations away from a straight configuration:

$$\mathrm{Wr}=\frac{1}{4\pi}\int ds\hat{\mathbf{z}}\cdot\mathbf{u}\times\frac{d\mathbf{u}}{ds}+\mathcal{O}(u^4) \quad (35)$$

This quantity is quadratic in **u** since the writhe of a straight line configuration is zero.

Using this in the twisting energy Eq. (33) and expanding to quadratic order in **u** gives:

$$\beta E=\frac{2\pi^2 C}{L}(\Delta\mathrm{Lk})^2-\beta f L+\int_0^L ds\left[\frac{A}{2}\left(\frac{d\mathbf{u}}{ds}\right)^2+\frac{\beta f}{2}\mathbf{u}^2-\frac{\pi C\sigma}{h}\hat{\mathbf{z}}\cdot\mathbf{u}\times\frac{d\mathbf{u}}{ds}\right] \quad (36)$$

which when Fourier transformed is

$$\beta E=\frac{2\pi^2 C}{L}(\Delta\mathrm{Lk})^2-\beta f L+\frac{1}{2L}\sum_q(\mathbf{u}_q^*)^T\begin{pmatrix}Aq^2+\beta f & -i(2\pi C/h)\sigma q\\ i(2\pi C/h)\sigma q & Aq^2+\beta f\end{pmatrix}\mathbf{u}_q \quad (37)$$

For the untwisted case $\sigma = 0$ this reduces to the fluctuation free energy of the untwisted chain, Eq. (9).

In terms of Cartesian components of **u**, nonzero twisting leads to an off-diagonal coupling, which can lead to a zero eigenvalue and an elastic instability. The stability condition is the requirement of a positive determinant $(Aq^2 + \beta f)^2 - (2\pi C/h)^2\sigma^2 q^2 > 0$. The eigenvalue vanishing condition occurs for σ_c satisfying $(2\pi C/h)^2\sigma_c^2 = 4\beta A f$. This instability places a

hard limit on the maximum value of σ^* for which this type of model can be applied; for f = 0.5 pN, this is $\sigma_c \approx 0.028$. By expressing this in terms of the DNA torque for a straight molecule $\tau = k_B T(2\pi C/h)\sigma$ we obtain $\tau_c^2 = 4k_B TAf$, which is the classical buckling instability of a rod subject to tension and torque [88]. The same instability can be observed in dynamical models of twisted and stretched DNA [89].

Diagonalization [9] of Eq. (37) allows computation of $\langle \mathbf{u}^2 \rangle$ and the free energy, in a Gaussian approximation. The extension is $\langle \mathbf{t}\cdot\hat{\mathbf{z}} \rangle = 1 - \langle \mathbf{u}^2 \rangle/2 + \mathcal{O}(u^4)$, or

$$\frac{\langle z \rangle}{L} = 1 - \sqrt{\frac{k_B T}{4Af}} - \frac{1}{2}\left(\frac{2\pi C}{h}\sigma\right)^2 \left(\frac{k_B T}{4Af}\right)^{3/2} + \dots \quad (38)$$

where the neglected terms are of higher order in $1/f$. Changing σ from zero leads to additional shrinkage over the untwisted case, due to chiral bending fluctuations.

Either integration of the extension with force, or direct computation of the partition function gives the free energy per length in a similar $1/f$ expansion:

$$\frac{\beta F}{L} = -\frac{\ln Z}{L} = -\beta f + \sqrt{\frac{f}{k_B TA}} + \frac{2\pi^2 C}{h^2}\left[1 - \frac{1}{2}\frac{C}{A}\left(\frac{k_B T}{4Af}\right)^{1/2}\right]\sigma^2 \quad (39)$$

The last term shows that the effect of the chiral fluctuations is to, as for DNA supercoiling, partially screen the twist energy, generating a reduction in the effective twist modulus $C \to C_f = C[1 - (C/2A)(k_B T/4Af)^{1/2}]$. This effect was used by Moroz and Nelson [83] to estimate the twist elastic constant C from single-molecule data of Strick et al [85] and led to a substantial revision in the accepted value of C from 75 nm up to the range 100 to 125 nm.

4.1.6. Coexistence of supercoiled and twisted-stretched DNA—For fixed force and sufficient ΔLk, one has “phase coexistence” of domains of plectonemic supercoiling and exended DNA (sketched in Fig. 10) [76, 77, 82, 39]. These “pure” states can be described by free energies per B-DNA length dependent on applied force f and the linking number density σ, say $\mathcal{S}(\sigma)$ for stretched and $\mathcal{P}(\sigma)$ for plectonemic DNA (the free energies per length discussed in the prior two sections, *i.e.*, up to a factor of $k_B T$, Eqs. (39) and (31)). For these pure states, the rate that work is done injecting linking number is proportional to torque, for example:

$$\tau = \frac{1}{\omega_0}\frac{\partial \mathcal{S}(\sigma)}{\partial \sigma} \quad (40)$$

The prefactor $\omega_0 = 2\pi/h = 2\pi/(3.6\text{ nm})$ is the angle of twist per molecule length for relaxed B-DNA, which converts the σ derivatives to ones with respect to angle.

[9] The eigenvectors of the matrix in Eq. (37) are proportional to the “circularly polarized” states $[1, \pm i]$

Along a molecule which is a fraction x_s of state S and fraction $x_p = 1 - x_s$ of state $\mathcal{P}$, the free energy per base pair of the mixed phase is

$$\mathcal{F}(\sigma)=x_{\mathrm{s}}\mathcal{S}(\sigma_{\mathrm{s}})+x_{\mathrm{p}}\mathcal{P}(\sigma_{\mathrm{p}}) \quad (41)$$

The equilibrium length fraction x_s and the free energy is determined by minimization of this free energy subject to the constraint $\sigma = x_s\sigma_s + x_p\sigma_p$: linking number is considered as being *partitioned* between the two states. In the case of interest here, the plectonemic regions are essentially closed loops (see Fig. 10). By "pinching" of those loops off to form circular plectonemic supercoils separated from the extended DNA, the calculation of writhe can be decoupled into separate writhes for extended and plectonemic regions.

If the pure state free energy densities plotted as a function of linking number density never cross, then one pure state or the other will be the equilibrium state, *i.e.*, one of the two extreme cases $x_s = 0$ or $x_s = 1$ will always minimize Eq. (41). If the two free energy densities cross, then there will be a range of σ over which there will be coexisting domains of the two states. Fig. 11 shows this situation, sketched to correspond to the case of main interest here, where at low values of σ the stretched state is stable (lower in free energy) relative to the plectoneme state, but where at large σ the stability reverses due to "screening" of the twist energy by the plectonemic state's writhe [76, 21, 39].

Minimization of Eq. (41) leads to a double-tangent construction familiar from other examples of phase coexistence (e.g., liquid-gas); in this case the conserved density is that of linking number (Fig. 11). The two coexisting states of linking number densities σ_s and σ_p satisfy $\partial\,\mathcal{S}(\sigma_s)/\partial\sigma_s = \partial\,\mathcal{P}(\sigma_s)/\partial\sigma_p$, *i.e.*, they have equal torques. They mix in proportions x_s and x_p, so the free energy in the coexistence region is

$$\mathcal{F}(\sigma)=\mathcal{S}(\sigma)+\frac{\partial\mathcal{S}(\sigma_{\mathrm{s}})}{\partial\sigma_{\mathrm{s}}}(\sigma-\sigma_{\mathrm{s}})=\mathcal{P}(\sigma)+\frac{\partial\mathcal{P}(\sigma_{\mathrm{p}})}{\partial\sigma_{\mathrm{p}}}(\sigma-\sigma_{\mathrm{p}}) \quad (42)$$

In the coexistence region, the fractions of the two states in the mixed state depend linearly on σ, as

$$x_{\mathrm{s}}=\frac{\sigma_{\mathrm{p}}-\sigma}{\sigma_{\mathrm{p}}-\sigma_{\mathrm{s}}} \quad x_{\mathrm{p}}=\frac{\sigma-\sigma_{\mathrm{s}}}{\sigma_{\mathrm{p}}-\sigma_{\mathrm{s}}} \quad (43)$$

The coexistence construction guarantees that the free energy is a convex function of linking number, and therefore that the torque is a monotonic function of linking number, as required for mechanical stability. In the coexistence region (σ between the limits σ_s and σ_p) the torques in the two types of domains are equal and σ-independent; *i.e.*, the σ-derivative of Eq. (42) is constant. This is quite useful for experiments on topoisomerases, since measurements carried out in the rather broad plectoneme-extended coexistence regions (along the linear portions of the "hat" curves of Fig. 12) are done at fixed torque. The value of torque in the coexistence regions is controlled by the constant force, varying from about 7 pN·nm at 0.5 pN (approximately the torque in a plasmid with physiological supercoiling $\sigma \approx 0.06$ [82,

60], to a little more than 25 pN·nm at 3 pN [82, 90] (note that there is an appreciable torque decrease with increased salt [60], since DNA hard-core diameter drops and therefore plectoneme tightness increases [81] with increased salt concentration).

In the coexistence region Eq. (43) indicates that the rate of change of the length fractions with σ is constant; $\partial x_s/\partial\sigma = -1/(\sigma_p - \sigma_s)$. This generates the linear dependence of molecule extension on linking number observed experimentally once the threshold for generating plectonemic DNA is reached, as can be seen by computing the molecule extension (as a fraction of relaxed double helix contour length L):

$$\frac{z}{L} = -\frac{\partial \mathscr{F}}{\partial f} = -x_s \frac{\partial \mathscr{S}(\sigma_s)}{\partial f} - x_p \frac{\partial \mathscr{P}(\sigma_p)}{\partial f} \quad (44)$$

In the coexistence region, the only σ dependence is the linear variation of x_s and x_p, making the dependence of extension on σ linear, a feature seen clearly in single-molecule experiments [60]. A series of extension versus σ curves computed as in Ref. [39] are shown in Fig. 12 to illustrate this. These are computed for the extended-state free energy per length, Eq. (39), and for the result of the plectoneme model of Eq. (31) [77, 81, 78, 39]. One alternately can use an approximate "harmonic" free energy model of the plectonemic phase, $\beta \mathscr{P}(\sigma) = (2\pi^2 C_p/h^2)\sigma^2$, where $C_p \approx 25$ nm which permits analytical computations of the phase diagram, see Ref. [82].

In the main case of interest here where $\mathscr{P}$ is the plectonemic supercoil state, its zero length eliminates its contribution to Eq. (44) (*i.e.*, $\partial \mathscr{P}/\partial f = 0$), yielding

$$\frac{z}{L} = -x_s \frac{\partial \mathscr{S}(\sigma_s)}{\partial f} = \frac{\sigma_p - \sigma}{\sigma_p - \sigma_s} \frac{z(\sigma_s)}{L} \quad (45)$$

where the final extension per length factor is the extension per length of the extended DNA state.

Experimentally, σ_s and σ_p may be measured from the beginning and the end of the linear coexistence regime of extension as a function of σ. Likewise, $z(\sigma_s)/L$ is the extension per length of the molecule at the onset of the linear regime. Thus Eq. (45) can be used to determine the coexisting state linking number values, the extension of the stretched DNA state as a function of force and linking number, and via integration, the free energy of the stretched state. Then through use of the tangent construction (Fig. (11)), the free energy of the plectonemic state can be measured. Note that when the molecule is entirely converted to plectoneme ($x_s = 0$, $x_p = 0$) the extension reaches zero. The point $\sigma = \sigma_p$ where this occurs can be estimated experimentally from extrapolation of extension data to zero.

As mentioned above, the phase-coexistence model generates torques which are constant along the linear regions of the "hat curves" of Fig. 12. For the model of Refs. [39] the extended-plectoneme coexistence torques are shown as a function of force in Fig. 13, and for a few salt concentrations (the models of Refs. [77, 81, 78] give very nearly the same results). There is a quite strong dependence of the torque on salt, due to electrostatic

repulsions limiting the tightness of plectoneme winding for lower salt, which tends to drive the torques higher. Interestingly the torque follows a power law $\tau \approx f^{0.72}$ in accord with experiment [60]; theoretically this is due to a $f^{3/4}$ dependence plus a logarithmic correction (Eq. 17 of Ref. [81], note $g(f) \approx f$ for $f \gg k_B T/A$).

An interesting aspect of experiments done on twisted DNA is that now one has an additional control parameter, ΔLk which can be used to construct thermodynamical "Maxwell relations" analogous to Eq. (21), but now involving torque $\langle \tau \rangle = \partial F/\partial(2\pi\Delta\mathrm{Lk})$ and force (and in principle, also chemical potential of molecules binding to the double helix) [58]. The Maxwell relation involving f and ΔLk has, for example, been used to indirectly measure torque, starting from extension-σ curves at a series of fixed forces [60] in reasonable accord with direct measurements [90].

Further interesting phenomena associated with twisted stretched DNA include the appearance of various structurally modified DNA states for sufficiently large twisting and force [39] (largely associated with torque-driven strand separation), appearance of multiple plectonemic domains for large molecules [78], and the discontinuous (first-order) nature of the onset of the plectonemic state [90].

4.2. Topoisomerases: protein machines that change DNA topology

In single-molecule DNA twisting experiments (as examples Refs. [85, 90, 60]), one changes the topology of the double helix (the value of ΔLk) by directly twisting the DNA molecule. In the cell, specialized enzymes (proteins that catalyze rearrangements of covalent bonds) allow double-helix topology to be changed. These *topoisomerases* cut and reseal the sugar-phosphate backbones in a double helix; depending on whether one or both backbones are cut, they are classified as type I or type II [91].

Type I topoisomerases do not require ATP for their operation, and just reversibly cut one backbone of the double helix, allowing it to rotate around the uncut strand, thus changing the ΔLk of a double helix. These enzymes therefore allow ΔLk of a DNA to reach mechanical-chemical equilibrium, which can be driven by *other* proteins acting on the double helix. In the absence of other factors acting on the double helix, type I topoisomerases therefore tend to *relax* $\Delta\mathrm{Lk} \to 0$. At present there are three subclasses of type I topoisomerases, which differ in details of their structures and their mechanisms [91]. The most important distinction is between type IA and IB, the former accomplishing a change in ΔLk = +1 per backbone cut-reseal catalytic cycle, and the latter changing ΔLk by one or more turns per catalytic cycle. Type I topos also can act on separate DNA molecules, typically in *decatenation* (disentanglement) of entangled single-stranded DNAs [92].

Type II topoisomerases cut *both* strands of a double helix, making a gap through which a second double helix is passed. Type II topos do this *once* per reaction cycle, and require ATP for this (the requirement of ATP appears to ensure that the second molecule is passed through the gap in a specific direction). This type of operation is essential to the removal of *entanglements* of separate DNA molecules. If a type II topo makes this topology change on two DNA molecules, the result is a change of the sign of a crossing (as in the two crossings shown in Fig. 7). Therefore the total number of crossings changes by ±2, and so the linking

number of the two molecules changes by ±1. To avoid confusion with ΔLk, the linking number of two separate double helices is called *catenation number* Ca. Thus type II topoisomerases are able to change the Ca of two DNAs by ±1. An important example of a type II topoisomerase is Topo IIα, which is the main enzyme acting to remove entanglements between DNAs in eukaryote cells[10].

Type II topoisomerases can also act at two points along a *single* DNA molecule. When this happens, there are *two* crossings of single strands inside the double helix which change sign, leading to a total change in ΔLk of the molecule being operated on by ±2. Bacteria contain a type II topoisomerase called *DNA gyrase* which is specially adapted for this function. This is thought to be accomplished the enzyme binding a +1-crossing loop, which then is changed in sign to −1. By this mechanism DNA gyrase is able to couple the energy stored in ATP into reduction of ΔLk to negative values (towards unwinding the double helix). DNA gyrase can drive $\sigma \to \approx -0.05$.

4.3. Linking of two double helices: DNA entanglement

Cells need to control the topology of very long DNA molecules. One can ask how DNA topology will change when topoisomerases are allowed to act on them, and how interactions with *other* proteins might be used to control DNA entanglement topology. The enzymes acting in a cell cannot directly sense entanglement or other nonlocal topological properties of chromosomes, and the mechanisms of DNA entanglement control are only starting to be understood.

4.3.1. Knots—A single circular molecule is in one of many possible *knotted* states. We can imagine having an ensemble of circular polymers which are allowed to slowly change their topology, so as to have equilibrated knotting topology (this is possible to achieve using topoisomerases, or using enzymes that alternately linearize and recircularize the molecules). We can ask what the probability P_{unknot} is that any molecule will be unknotted.

One might ask how P_{unknot} behaves with the length L of the circles. For small L, (more precisely for $L/b < 1$ where b is the segment length; recall $A = b/2$ and $N = L/b$) there will be a large free energy cost of closing a molecule into a knot, driving $P_{\text{unknot}} \to 1$. One can argue that for large L, $P_{\text{unknot}} \approx \exp[-L/(N_0 b)]$, for some constant N_0 as follows. Over some polymer length N_0 segments we suppose that the probability of having no knot drops to $1/e$. Applying this probability to each L_0 along a DNA of length L gives $P_{\text{unknot}}(L) \approx (1/e)^{L/(N_0 b)}$. This rough argument can be made mathematically rigorous[93].

Remarkably, even for an 'ideal' polymer which has no self-avoidance interactions, $N_0 \approx 300$; for a slightly self-avoiding polymer like dsDNA in physiological buffer, $N_0 \approx 400$ [94]. What this means is that to have an appreciable probability $(1 - 1/e)$ to find even one knot along a dsDNA, it has to be $400 \times 300 = 120,000$ bp long (the long persistence length of DNA - b contains 300 bp - helps make this number so impressive). The knotting length N_0 depends very strongly on self-avoidance; for a strongly self-avoiding polymer (meaning an excluded volume per statistical segment approaching b^3), $N_0 \approx 10^6$. The remarkably low

[10]the corresponding enzyme in bacteria is called Topo IV

probability of polymer knotting lacks fundamental understanding, being based on numerical simulation results[94].

Experiments on circular DNAs are in good quantitative agreement with statistical mechanical results for the semi-flexible polymer model including DNA self-avoidance interactions. For example, it is found that the probability of finding a knot generated by thermal fluctuations for a 10 kb dsDNA is about 0.05 both experimentally and theoretically [95, 1]. This can be interpreted thermodynamically; the free energy of the knotted states relative to the unknotted state in this case is k_BT ln(0.95/0.05), or about $3k_BT$.

A remarkable experimental observation is that type II topoisomerases are by themselves able to push this probability down, by a factor of between 10 and 100[96]. Somehow topo II is able to use energy from ATP hydrolysis to actively suppress entanglements.

4.3.2. Suppressing knotting by lengthwise compaction—Having a formula for the unknot probability, $P_{\text{unknot}}(L) = e^{-L/(N_0 b)}$ gives some insight into a mechanism by which locally acting enzymes could control global DNA topology. Consider a long dsDNA of length L, in the presence of some proteins which act to fold DNA up along its length. Imagine that these proteins cannot ‘cross-link’ DNA segment but that they can only compact the molecule *along* its length (Fig. 14). As lengthwise-compacting proteins bind, we imagine that they modify the total contour length to be $L' < L$, and effective segment length to $b' > b$.

If these proteins bind slowly in the presence of type-II topoisomerases so that the knotting topology can reach close to equilibrium, then the unknotting probability will have the form $P_{\text{unknot}} = \exp[-(L'/b')/N_0]$. Therefore, gradually compacting (decreasing L') while stiffening (increasing b') DNA can drive knotting out of it. Unknotting (an example of “entanglement resolution”) will occur on progressively larger length scales as this compaction process proceeds [41].

4.3.3. Proteins that lengthwise-compact DNA—Actual chromosomes in cells *are* substantially lengthwise-compacted by the action of locally-acting DNA-binding proteins. In eukaryotes, histone protein octamers wrap 147 bp of dsDNA into nucleosomes about 10 nm in diameter [48]. Chromosomal DNAs typically have short (15 to 50 bp) “linker” DNA stretches between successive nucleosomes. It is presently thought that a persistence length of this type of “chromatin” fiber contains at least 10 nucleosomes, or about 2 kb of DNA. This means that even with no self avoidance, a knot in an isolated chromatin fiber will only become likely for an 800 kb segment (4000 nucleosomes). In a cell, additional proteins that mediate chromatin-chromatin contacts will keep the statistics of the fibers from being those of simple polymers at very large scales, but there should still be a strong knotting suppression by the folding of DNA by architectural proteins.

At larger scales, chromosomes are folded and compacted by other proteins. One of the most important classes of proteins which accomplish this are “Structural Maintenance of Chromosomes” (SMC) complexes (Fig. 15) [97, 98, 99, 100]. These protein complexes are based on heterodimers of SMC proteins, which are long (≈ 50 nm), stick-like coiled-coil proteins with a dimerization domain at one end and an ATP-binding/hydrolyzing domain at

the other end. These SMC "sticks" dimerize at one end, and are thought to be capable of undergoing conformational changes in response to ATP binding and hydrolysis so as to compact DNA molecules that they are interacting with. Via interactions with a third "kleisin" protein, SMC dimers form a tripartite ring structure that can encircle DNA, indicating a topological element to their DNA-organizing functions [101, 102, 103]. Furthermore, eukaryote SMCs appear to favor formation of *right-handed* DNA loops (loops with positive DNA writhe) [104, 105, 106, 107].

Single-molecule experiments do indicate that SMC complexes can compact DNA molecules by mediating contacts between distant DNA loci [108, 109, 110, 107]. Cell-biological experiments indicate clearly that the lengthwise compaction that occurs during mitosis in eukaryote cells depends crucially on the presence of "condensin" SMCs [98], and that proper regulation of contacts ("cohesion") between replicated DNAs depends on "cohesin" SMCs [97, 100]. Cohesins also appear to play a critical role in stabilizing gene-regulating loops along chromosomes in eukaryotes. SMC complexes are found in bacteria and archae [111], making SMCs the most universal class of DNA-folding proteins, present in all three domains of life.

4.3.4. Linking of two "tandem" circular DNAs—The simplest topological problem involving more than one circular polymers involves the level of linking between two chain molecules. As a DNA is replicated, one often encounters the situation where the two duplicate molecules are attached together at a point along their contours. This situation suggests the problem of the computation of the catenation number statistics for two long circular polymers each N statistical segments long, attached together at one segment (Fig. 16).

The catenation number Ca is just the Gauss invariant, Eq. (24), of the two polymers, and is the sum of signed crossings (Fig. 7). Therefore we expect $\langle \mathrm{Ca} \rangle = 0$; right- and left-handed crossings occur with similar probabilities. However, the *width* of the Ca distribution, $\langle \mathrm{Ca}^2 \rangle$ will be nonzero, and at least as large as the number of *nearby* crossings, since those close crossings will appear with either sign in the conformational ensemble.

We can estimate the number of nearby crossings for ideal random-walk polymers using the segment density of $\varphi \approx 1/N^{1/2}$, which tells us $\langle \mathrm{Ca}^2 \rangle \approx N\varphi \approx N^{1/2}$. This suggests a scaling law of

$$\langle \mathrm{Ca}^2 \rangle = a_0 N^{1/2} \quad (46)$$

or $|\mathrm{Ca}| \approx N^{1/4}$. This scaling behavior has been suggested by des Cloixeau[112] and calculated by Tanaka[113]; numerical simulations for ideal random walks suggest $a_0 \approx 0.25$ [114].

This fluctuation scaling indicates a free energy cost of catenations of $F(\mathrm{Ca}) \approx k_B T \mathrm{Ca}^2 / \langle \mathrm{Ca}^2 \rangle$, or $F(\mathrm{Ca}) \approx k_B T \mathrm{Ca}^2 / N^{1/2}$. Since *Ca* is extensive, the free energy is superextensive; if we scale Ca up with polymer length ($L = Nb$), we see $F \approx L^{3/2}$. Comparing this to the form of the twist elasticity for an elastic rod Eq. (25), we see that the effective twist persistence

length diverges with polymer length, $C_{\rm eff} \approx L^{1/2}$ (this divergence is due to the large entropy cost of forcing two otherwise conformationally unconstrained polymers to wrap one another).

If one has excluded volume interactions along two polymers that are tethered together, the number of nearby crossings drops to $O(1)$ [115], and no longer dominates over the $\approx \ln N$ number of crossings that comes from nonlocal wrapping of the polymers around one another. The $\ln N$ arises simply because each successive nonlocal wrap requires an additional increment of chainlength $\approx N$, making $d\mathrm{Ca}^2/dN \approx 1/N$. [11] Simulations verify this [114], showing that for polymers with excluded volume

$$\langle \mathrm{Ca}^2 \rangle \approx a_1 \ln N \quad (47)$$

with a_1 dependent on the excluded volume of the polymer segments.

A consequence of this low fluctuation is a high stiffness; for small Ca, the free energy of catenation will be $F(\mathrm{Ca}) \approx k_B T \mathrm{Ca}^2/(a \ln N)$. The higher cost of catenations in the self-avoiding case (relative to the ideal random walk case) gives rise to a more strongly diverging effective elastic constant, $C_{\rm eff} \approx L/\ln L$. This large cost of interwindings can be expected to lead to "phase separation" of loose and tight catenations. In simulations one observes a sign of this in a nearly *linear* dependence of $F(\mathrm{Ca})$ on Ca, with a cost of about $4k_BT$ per catenation over a wide range of catenation [114]. A key point is that in this nonlocally wrapped structure, most of the catenations will be located where the chains are near one another, *i.e.*, near the tethering point of the two chains.

Catenations between either ideal or self-avoiding polymers have a high free energy cost. This can be argued to give some insight into the origin of the knotting length N_0 since the simplest "trefoil" knot involves the wrapping of a polymer around itself, with at least three crossings [114]. This also indicates that catenations between *isolated* DNAs will be disfavored; type II topoisomerases can be expected to reduce catenation down to the thermal levels of $\langle \mathrm{Ca}^2 \rangle$ discussed above (this ignores any ATP-driven topological simplification effects which type II topos may possess [96].

Lengthwise compaction of polymers as discussed above for knots will drive out catenations. For both ideal and self-avoiding polymers, changing $N \rightarrow N' < N$ will increase the free energy cost of Ca, guiding topoisomerases to remove catenations.

The tendency for interwindings to "condense" together will tend to drive the helical catenations resulting from DNA replication to be near one another. Along chromosomes which are attached together at a point, one can expect a domain of tight catenation, on which type II topoisomerases can be expected to act to release the catenations. The $4k_BT$ per catenation expected in such a structure will strongly bias catenation release.

[11] At the Nth monomer position, the chain ends are some average distance $R(N)$ away from one another. The *next* crossing can be expected only after an additional N monomers along the chains, allowing the chain ends to transit the distance R. This indicates the rate of increase of the number of crossings with chainlength is $\propto 1/N$. This scaling is independent of how R increases with N (i.e., on the Flory exponent $\nu \approx 0.6$ in $R(N) \approx N^{\nu}$) but does require self avoidance, to suppress the contribution from nearby crossings [114].

4.3.5. Linking of confined polymers—The two examples discussed above - knotting of one polymer and catenation of two polymers tethered together at one point - both indicate that entanglements cost a good deal of free energy, but these were cases of isolated polymers. We now consider entanglements between n polymers each of N segments, in a dense melt- or semi-dilute-solutionlike state, confined to a radius-R spherical cavity [12]. The polymers are long enough so that their random-walk size $N^{1/2} \gg R$, so that each chain fills the confinement volume. This is a crude model of chromosomes confined to a nucleus, or inside a bacterial cell.

We now ask what the degree of catenation will be if the entanglement topology of these confined chains is equilibrated (for example by topoisomerases). For a polymer melt, along a chain of N segments, every segment is nearby other segments (not counting the segments to the left and right along the same chain). Most of these near encounters are with segments from *other* chains, since the number of collisions of a chain with itself is $\approx N^{1/2}$ for the random-walk statistics in a melt. This means that each chain has N near collisions with other chains, or N/n near collisions with any particular chain. But since these near collisions appear in the ensemble of configurations with either crossing sign, we expect $\langle \mathrm{Ca}^2 \rangle \approx N/n$. For this problem, the high segment density and the proximity of the polymers to one another forces them to be much more entangled than isolated chains.

In the semi-dilute solution case (volume fraction $\varphi = nNb^3/R^3 \ll 1$ but with overlapping chains), exactly the same argument can be made, but now for semi-dilute solution blobs, which each have $g \approx \varphi^{-5/4}$ segments in them. The result is that $\langle \mathrm{Ca}^2 \rangle = \varphi^{5/4} N/n$. Simulations indicate that the two regimes can be described by one scaling formula (Fig. 17) [116]

$$\langle \mathrm{Ca}^2 \rangle = \frac{N}{n} c(\phi) \quad (48)$$

where f is a scaling function with limiting behaviors $c(\varphi) \propto \varphi^{5/4}$ for $\varphi \ll 1$, and $c(\varphi) \to$ const for $\varphi \to 1$.

Once again one can see that lengthwise compaction so as to reduce $N = L/b$ (by either or both of reduction of chromosome length L or increase of segment length b, while keeping φ about the same) will drive down $\langle \mathrm{Ca}^2 \rangle$.

An interesting issue is the influence of the shape of the volume on entanglement of confined polymers. For tight cylindrical confinement, chains will tend to separate from one another along the cylinder, to minimize their stretching (and therefore to maximize their entropy). This effect has been proposed to play a role in the segregation of bacterial chromosomes in

[12]Considering the polymers to be circular makes the concept of Ca precisely defined, but this is not essential since closing each chain with a straight segment introduces subleading contributions to the scaling results discussed here. For example, for two overlapping random walks of size $r \approx N^{1/2}b$, a straight-line closure generates $\approx r\varphi/b$, where φ is the segment volume fraction. Given $r \approx N^{1/2}b$ and $\varphi \approx N^{-1/2}$ we see that the closure generates only $O(1)$ additional crossings, a small fraction of the $\approx N^{1/2}$ crossings generated by the chains. Similar estimates indicate that confined polymers have the same property.

rod-shaped bacteria[117, 118] although folding and compaction of bacterial chromosomes (Fig. 18) likely play an important role in their separation [119].

4.4. Estimate of equilibrium entanglement for human chromosomes

Given a scaling theory for equilibrium linking for confined polymers, one can estimate the thermal equilibrium entanglement using Eq. (48) that would occur for otherwise unconstrained chromosomes within a cell nucleus, under the assumptions that random strand passages are made by type-II topoisomerases, and that the chromosomes behave as self-avoiding polymers [116].

A statistical segment of chromatin is thought to be roughly $b = 60$ nm in length[120], and considering it to be a well-packed fiber about 30 nm wide, contains about 35 nucleosomes or 6 kb of DNA. Thus, the larger human chromosomes, approximately 200 Mbp in length, as chromatin correspond to $N \approx 30{,}000$ segment-long polymers. Human chromosomes are confined within a cell nucleus of radius $R \approx 3\ \mu$m, or measured in polymer segment units, $R/b = 50$. The number of chromosomes in a human nucleus is $n = 46$, thus we can compute the segment density $\varphi = nN/(R/b)^3 = 10$, corresponding to a volume fraction of roughly 10%. Reading off $\langle Ca^2\rangle/(N/n) = 0.06$ for this φ value from Fig. 17 gives the estimate $\langle Ca^2\rangle_0 = 40$. This is likely an overestimate since chromatin fiber has a segment diameter-to-length ratio larger than the $b/d = 0.2$ used to compute Fig. 17. In conclusion, if human chromosomes were to fully equilibrate their topology, they would be expected to have $\langle Ca^2\rangle \approx 40$; *i.e.*, they would equilibrate to an entangled state. The value of $\langle Ca^2\rangle$ is much smaller than N in numerical size.

It is to be stressed that $\langle Ca^2\rangle_0$ is not necessarily the actual catenation that occurs in the cell, but only that which would occur if topology were equilibrated for uncondensed chromosomes in a nucleus. It has been estimated that the time needed for topological equilibrium may greatly exceed cell-cycle timescales, and that observations of chromosome territories (distinct spatial regions of the nucleus that contain separate chromosomes) may be related to this kinetic constraint [121]. Other factors such as tethering of chromosomes to the nuclear envelope during interphase [121], or formation of condensed heterochromatin domains, likely play a major role in maintaining chromosome territories and limiting chromosome entanglement. Nevertheless, the estimate $\langle Ca^2\rangle_0$ is useful as it is a thermodynamic upper bound on entanglement of chromosomes confined to a nucleus.

4.5. Lengthwise compaction and control of chromosome entanglements

During cell division, eukaryote chromosomes become completely segregated from one another, despite the fact that following DNA replication, the chromosomes are released from being tethered to the inside of the nuclear envelope, and have an opportunity to entangle with one another [122]. Evidence for inter-chromosome entanglements have been obtained from experiments in fission yeast where the DNA-topology-changing enzyme topo II was disabled during chromosome condensation: *different* chromosomes were observed to be unable to segregate from *one another* [123]. Similar effects have been observed *in vitro* in experiments with *Xenopus* egg extracts [124], and *in vivo* for mammalian cells [125, 126]. These observations of inter-chromosome entanglements following suppression of topo II

activity imply that chromosomes became entangled with one another at some time prior to the inhibition.

Strikingly, following DNA replication, chromosomes start to *condense* into string-like structures that become gradually visible in the light microscope (Fig 19, also see Ref. [122]). This process of "chromosome condensation" is thought to be coupled to the process of segregation of chromosomes from one another [127, 128, 129, 122] as well as to separation of sister chromatids from one another inside each chromosome The peculiar type of "condensation" that occurs - "lengthwise compaction", or folding of chromosomes along their length - ensures separation of different chromosomes, provided that topo II is present during the compaction process This should be contrasted with the manner of condensation discussed in polymer physics ("poor solvent" or "polymer melt" conditions) whereby all segments stick to one another; if this occurred to chromosomes they would become hopelessly entangled with one another, as occurs in a polymer melt [130].

Eq (48) can be used to show how lengthwise compaction can drive segregation of different chromosomes even while confined inside the nucleus. Consider chromosomes which are initially in the form of flexible polymers of N statistical segments each of b and cross-sectional diameter d. Suppose lengthwise compaction occurs: the chromosomes will become locally thicker ($d \rightarrow d' > d$) but in doing so will become stiffer ($b \rightarrow b' > b$) and shorter ($L = Nb \rightarrow L' = N'b' < N$) A simple and reasonable assumption is that the condensation process will conserve chromatin volume *i.e.* $Ld^2 = L'd'^2$ or $Nbd^2 = N'b'd'^2$. To simplify the calculation to follow it will be assumed that as condensation occurs b and d will increase by the same factor, *i.e.*, $b' = \lambda b$ and $d' = \lambda d$. For this particular model the volume conservation constraint indicates $N' = N/\lambda^3$. This simple model of chromosome condensation describes the degree of condensation by the single parameter $\lambda > 1$.

As chromosome condensation occurs λ gradually increases, and by Eq. (48) the equilibrium catenation of chromosomes will be

$$\langle \mathrm{Ca}^2 \rangle_\lambda = \frac{N'}{n} c([nN'b'^3]/R^3) = \frac{1}{\lambda^3}\frac{N}{n} c([nNb^3]/R^3) = \frac{1}{\lambda^3}\langle \mathrm{Ca}^2 \rangle_0 \quad (49)$$

where $\langle \mathrm{Ca}^2 \rangle_0$ is the catenation that would be achieved in topological equilibrium *before* chromosome condensation begins (the estimate made above for human chromosomes)

The level of entanglement of chromosomes need not initially be close to $\langle \mathrm{Ca}^2 \rangle_0$ for Eq. (49) to apply during chromosome condensation Eq. (49) indicates the equilibrium catenation that can be reached, assuming random strand passages by topoisomerase II, given lengthwise condensation by a factor λ, and shows how lengthwise compaction can generate a strong thermodynamic drive to eliminate catenations between different chromosomes. The interactions that accomplish local condensation of chromosomes by a factor λ suppress the equilibrium level of entanglement $\langle \mathrm{Ca}^2 \rangle$ by a factor λ^{-3}.

Therefore, the equilibrium catenation expected for uncondensed human chromosomes, $\langle \mathrm{Ca}^2 \rangle = 40$, can be pushed well below 1 by only moderate condensation $\lambda = 6$. By locally folding

chromatin fiber from its uncondensed level (30 nm thickness) to a lengthwise-compacted 200 nm-thick fiber will ensure complete decatenation of different chromosomes. The increase of b and d by the same factor λ allows the same scaling function $c(\varphi)$ to be used which simplifies this computation, but this condition is not required to obtain the same condensation-driven topological resolution. Finally, it should be noted that the segment density is unchanged by this condensation process, but the total number of segments per chain is reduced by a factor λ^3; for the human chromosome case considered above ($\lambda = 6$) $N' = N/\lambda^3 \approx 30{,}000/200 \approx 150$. Thus, when human chromosomes become separated by this process, they will still be relatively long, flexible polymers.

At the same time that the chromosomes are being separated from one another, the chromatids will separate, via the same general mechanism but now using Eqs. (46) and (47) applied to tandem stretches of chromatin between chromatid cohesion points [129].

To summarize, the mechanism outlined here of lengthwise-compaction-driven entanglement removal requires that there first be enzymes which act to fold chromatin along its length, without introduction of extensive “cross-links” between different chromosomes. Then, this compaction system must act slowly enough that there is time for topology-changing enzymes (topo II) to release entanglements between different chromosomes. Given these two requirements, as lengthwise compaction goes forward, entanglements will be released at successively large length scales by the combined action of the lengthwise compaction mechanism and topo II.

In accord with this, disturbing either the compaction or topology-changing machinery has been observed to disrupt the condensation-resolution process [123, 124, 125, 126, 98, 131]. Finally, fully condensed chromosomes become “individualized” (lengthwise compaction can generate this as well, see Ref. [114]), and following separation of sister chromatids, the two sets of replicated chromosomes then decondense to form nuclei. As emphasized by Rosa and Everaers[121] kinetic effects may delay full re-entanglement, giving time for establishment of chromosome tethering and other nuclear structures factors stabilizing chromosome territories.

5. Conclusion

These lectures have introduced statistical-mechanical models that can be used to describe the polymer elasticity of DNA and other biological polymers. Methods have been discussed for including effects of DNA-binding proteins into these models. Many more problems, particularly concerning the kinetics associated with DNA-binding proteins, remain to be studied. This paper has emphasized the importance of considering the multi-step kinetics associated with the array of chemical bonds between a typical DNA-binding protein and its binding site.

A few problems associated with the topology of DNA molecules have also been described. The simplest of these concerns the supercoiling of DNA, or the response of a single DNA to perturbation of its internal linking number. The more complex problem of entanglement of separate DNA molecules (or chromosomes) has been discussed, mainly in terms of the

width of the catenation number distribution, $\langle Ca^2 \rangle$, which is a simple and useful tool for gauging the entanglement in multi-polymer systems.

This approach has been used to rationalize how chromosome condensation - or better put "lengthwise compaction" of chromosomes - can lead to topological simplification and chromosomes separation. The key idea has been to consider topo II as a "topology-changing machine" which needs to be *directed* by a "lengthwise-compaction machine". The free energy drive to direct topo II to remove entanglements comes from the free energy associated with chromosome lengthwise compaction. Some preliminary ideas of how specific chromosome-structuring proteins (specifically the "condensin" chromatin-folding complex) might accomplish this are described in Ref. [132]. Single-molecule studies of condensin and other "SMC" (Structural Maintenance of Chromosome) proteins are of obvious interest; single-DNA experiments have demonstrated DNA-folding capabilities of condensin and cohesin complexes [108, 107].

Acknowledgments

This work was supported by NSF grants MCB-1022117, DMR-1121262 (NU-MRSEC) and DMR-1206868, and by NIH grants U54CA143869-01 (NU-PS-OC) and R01GM105847.

References

1. Rybenkov VV, Cozzarelli NR, Vologodskii AV. Proc Natl Acad Sci USA. 1993; 11:5307. [PubMed: 8506378]
2. Goodsell, DS. The machinery of life. Springer-Verlag; New York: 1992.
3. Swinger KK, Lemburg KM, Zhang Y, Rice PA. EMBO J. 2003; 22:3749. [PubMed: 12853489]
4. Grindley NDF, Whiteson KL, Rice PA. Ann Rev Biochem. 2006; 75:567. [PubMed: 16756503]
5. Taneja B, Patel A, Slesarev A, Mondragon A. EMBO J. 2006; 25:398. [PubMed: 16395333]
6. Luger K, Mader AW, Richmond RK, Sargent DF, Richmond TJ. Nature. 1997; 389:251. [PubMed: 9305837]
7. Grandbois M, Beyer M, Rief M, Clausen-Schaumann H, Gaub HE. Science. 1999; 283:1727. [PubMed: 10073936]
8. Krasnoslobodtsev AV, Shlyakhtenko LS, Lyubchenko YL. J Mol Biol. 2007; 365:1407. [PubMed: 17125791]
9. Marko JF, Siggia ED. Biophys J. 1997; 73:2173. [PubMed: 9336213]
10. Sankararaman S, Marko JF. Phys Rev E. 2005; 71:021911.
11. Blumberg S, Tkachenko AV, Meiners JC. Biophys J. 2005; 88:1692. [PubMed: 15653717]
12. Yan J, Kawamura R, Marko JF. Phys Rev E. 2005; 71:061905.
13. Skoko D, Yan J, Johnson RC, Marko JF. Phys Rev Lett. 2005; 95:208101. [PubMed: 16384101]
14. Gemmen GJ, Millin R, Smith DE. Proc Natl Acad USA. 2006; 103:11555.
15. Chen YF, Milstein JN, Meiners JC. Phys Rev Lett. 2010; 104:048301. [PubMed: 20366742]
16. Wang MD, Schnitzer MJ, Yin H, Landick R, Gelles J, Block SM. Science. 1998; 282:902. [PubMed: 9794753]
17. Maier B, Bensimon D, Croquette V. Proc Natl Acad Sci USA. 2000; 97:12002. [PubMed: 11050232]
18. Hagerman PJ. Ann Rev Biophys Biophys Chem. 1988; 17:265. [PubMed: 3293588]
19. Doi, M.; Edwards, SF. Theory of Polymer Dynamics. Oxford University Press; New York: 1989. Sec. 8.8
20. de Gennes, PG. Scaling Concepts in Polymer Physics. Cornell University Press; Ithaca: 1979. Sec. I.4.1

21. Marko JF, Siggia ED. Macromolecules. 1995; 28:8759.
22. Neuman KC, Lionnet T, Allemand JF. Ann Rev Mater Res. 2007; 37:33.
23. SantaLucia J Jr. Proc Natl Acad Sci USA. 1998; 95:1460. [PubMed: 9465037]
24. Smith SB, Finzi L, Bustamante C. Science. 1992; 258:1122. [PubMed: 1439819]
25. Essevaz-Roulet B, Bockelmann U, Heslot F. Proc Natl Acad USA. 1997; 94:11935.
26. Bockelmann U, Thomen Ph, Viasnoff V, Heslot F. Biophys J. 2002; 82:1537. [PubMed: 11867467]
27. Lubensky DK, Nelson DR. Phys Rev Lett. 2000; 85:1572. [PubMed: 10970557]
28. Lubensky DK, Nelson DR. Phys Rev E. 2002; 65:031917.
29. Cocco S, Monasson R, Marko JF. Proc Natl Acad Sci USA. 2002; 66:051914.
30. Danilowicz C, Coljee VW, Bouziques C, Nelson DR, Prentiss M. Proc Natl Acad Sci USA. 2003; 100:1694. [PubMed: 12574500]
31. Cluzel P, Lebrun A, Heller C, Lavery R, Viovy JL, Chatenay D, Caron F. Science. 1996; 271:792. [PubMed: 8628993]
32. Smith SB, Cui Y, Bustamante C. Science. 1996; 271:795. [PubMed: 8628994]
33. Cocco S, Yan J, Leger JF, Chatenay D, Marko JF. Phys Rev E. 2004; 70:011910.
34. Strick, TR.; Bensimon, D.; Croquette, V. Structural Biology and Functional Genomics. Bradbury, EM.; Pongor, S., editors. Kluwer Academic; Boston: 1999. p. 87-96.NATO Science Series 3
35. Cocco S, Monasson R. Phys Rev Lett. 1999; 83:5178.
36. Sarkar A, Léger JF, Chatenay D, Marko JF. Phys Rev E. 2001; 63:051903.
37. Bryant Z, Stone MD, Gore J, Cozzarelli NR, Bustamante C. Nature. 2003; 424:338. [PubMed: 12867987]
38. Sheinin MY, Forth S, Marko JF, Wang MD. Phys Rev Lett. 2011; 107:108102. [PubMed: 21981534]
39. Marko JF, Neukirch S. Phys Rev E. 2013; 88:062722.
40. Halford SE, Marko JF. Nucl Acids Res. 2004; 32:3040. [PubMed: 15178741]
41. Marko, JF. Multiple aspects of DNA and RNA from biophysics to bioinformatics. Elsevier; 2005. Introduction to single-DNA micromechanics; p. 211-270.Les Houches Session LXXXII
42. Parsaeian A, de la Cruz MO, Marko JF. Phys Rev E. 2013; 88:040703R.
43. Mascotti DP, Lohman TM. Proc Natl Acad Sci USA. 1990; 87:3142. [PubMed: 2326273]
44. Mirny LA. Proc Natl Acad Sci USA. 2010; 107:22534. [PubMed: 21149679]
45. McGhee JD, von Hippel PH. J Mol Biol. 1974; 86:469. [PubMed: 4416620]
46. Léger JF, Robert J, Bordieu L, Chatenay D, Marko JF. Proc Natl Acad Sci USA. 1998:95, 12295. [PubMed: 9419334]
47. Forget AL, Kowalczykowski SC. Nature. 2012; 482:423. [PubMed: 22318518]
48. Killian JL, Li M, Sheinin MY, Wang MD. Curr Opin Struct Biol. 2012; 22:80. [PubMed: 22172540]
49. Rimsky S, Travers A. Curr Opin Microbiol. 2011; 14:136. [PubMed: 21288763]
50. Ali BMJ, Amit R, Braslavsky I, Oppenheim AB, Gileadi O, Stavans J. Proc Natl Acad Sci USA. 2001; 98:10658. [PubMed: 11535804]
51. van Noort J, Verbrugge S, Goosen N, Dekker C, Dame RT. Proc Natl Acad Sci USA. 2004; 101:6969. [PubMed: 15118104]
52. Skoko D, Wong B, Johnson RC, Marko JF. Biochemistry. 2004:43, 13867.
53. Skoko D, Yoo D, Bai H, Schnurr B, Yan J, McLeod SM, Marko JF, Johnson RC. J Mol Biol. 2006; 36:777. [PubMed: 17045294]
54. McCauley MJ, Rueter EM, Rouzina I, Maher III LJ, Williams MC. Nucl Acids Res. 2012; 41:167. [PubMed: 23143110]
55. Yan J, Marko JF. Phys Rev E. 2003; 68:011905.
56. Zhang H, Marko JF. Phys Rev E. 2010; 82:051906.
57. Xiao B, Zhang H, Johnson RC, Marko JF. Nucl Acids Res. 2011; 39:5568. [PubMed: 21427084]
58. Zhang H, Marko JF. Phys Rev E. 2008; 77:031916.

59. Liebensy P, Goyal S, Dunlap D, Family F, Finzi L. J Phys Condens Mat. 2010; 22:414104.
60. Mosconi F, Allemand JF, Bensimon D, Croquette V. Phys Rev Lett. 2009; 102:078301. [PubMed: 19257716]
61. Jacobson DR, McIntosh DB, Saleh OA. Biophys J. 2013; 105:2569. [PubMed: 24314087]
62. Rudnick J, Bruinsma R. Biophys J. 1999; 76:1725. [PubMed: 10096873]
63. Zhang H, Marko JF. Phys Rev Lett. 2012; 109:248301. [PubMed: 23368394]
64. Kim S, Brostromer E, Xing D, Jin J, Chong S, Ge H, Wang S, Gu C, Yang L, Gao YQ, Su XD, Sun Y, Xie XS. Science. 2013; 339:816. [PubMed: 23413354]
65. Xu X, Ge H, Gao YQ, Wang SS, Thio BJ, Hynes JT, Xie XS, Cao J. J Phys Chem B. 2013; 117:13378. [PubMed: 23795567]
66. Graham J, Marko JF. Nucl Acids Res. 2011; 39:2249. [PubMed: 21097894]
67. Loparo JJ, Kulczyk AW, Richardson CC, van Oijen AM. Proc Natl Acad Sci USA. 2011; 108:3584. [PubMed: 21245349]
68. Joshi CP, Panda D, Martell DJ, Andoy NM, Chen TY, Gaballa A, Helmann JD, Chen P. Proc Natl Acad Sci USA. 2012; 109:15121. [PubMed: 22949686]
69. Ha T. Cell. 2013; 154:723. [PubMed: 23953107]
70. Gibb B, Ye LF, Gergoudis SC, Kwon Y, Niu H, Sung P, Greene EC. PLOS One. 2014; 9:e87922. [PubMed: 24498402]
71. Sing CE, de la Cruz MO, Marko JF. Nucl Acids Res. 2014; 42:3783. [PubMed: 24393773]
72. Cocco S, Marko JF, Monasson R. Phys Rev E. 2014; 112:238101.
73. Vologodskii AV, Marko JF. Biophys J. 1997; 73:123. [PubMed: 9199777]
74. White JH. Am J Math. 1969; 91:693.
75. Fuller FB. Proc Natl Acad Sci USA. 1971; 68:815. [PubMed: 5279522]
76. Marko JF, Siggia ED. Science. 1994; 265:506. [PubMed: 8036491]
77. Marko JF, Siggia ED. Phys Rev E. 1995; 52:2912.
78. Marko JF, Neukirch S. Phys Rev E. 2012; 85:011908.
79. Helfrich W, Harbich W. Chem Scr. 1985; 25:32.
80. Burkhardt TW. J Phys A. 1997; 30:L167.
81. Neukirch S, Marko JF. Phys Rev Lett. 2011; 106:138104. [PubMed: 21517425]
82. Marko JF. Phys Rev E. 2007; 76:021926.
83. Moroz D, Nelson P. Proc Natl Acad Sci USA. 1997; 94:14418. [PubMed: 9405627]
84. Moroz JD, Nelson P. Macromolecules. 1998; 31:6333.
85. Strick TR, Allemand JF, Bensimon D, Bensimon A, Croquette V. Science. 1996; 271:1835. [PubMed: 8596951]
86. Fuller FB. Proc Natl Acad Sci USA. 1978; 75:3557. [PubMed: 16592550]
87. Neukirch S, Starostin EL. Phys Rev E. 2008; 78:041912.
88. Love, AEH. Treatise on the Mathematical Theory of Elasticity. Dover; New York: 1944. Sec. 264
89. Banigan EJ, Marko JF. Phys Rev E. 2014; 89:062706.
90. Forth S, Sheinin MY, Daniels B, Sethna JP, Wang MD. Phys Rev Lett. 2008; 100:148301. [PubMed: 18518075]
91. Koster DA, Crut A, Shuman S, Bjornsti MA, Dekker NH. Cell. 2010; 142:519. [PubMed: 20723754]
92. Terekhova K, Marko JF, Mondragon A. Biochem Soc Trans. 2013; 41:571. [PubMed: 23514156]
93. Sumners DW, Whittington SG. J Phys A Math Gen. 1988; 21:1689.
94. Koniaris K, Muthukumar M. Phys Rev Lett. 1991; 66:2211. [PubMed: 10043425]
95. Shaw SY, Wang JC. Science. 1993; 260:533. [PubMed: 8475384]
96. Rybenkov VV, Ullsperger C, Vologodskii AV, Cozzarelli NR. Science. 1997; 277:648. [PubMed: 9254431]
97. Strunnikov AV, Larionov VL, Koshland D. J Cell Biol. 1993; 123:1635. [PubMed: 8276886]
98. Hirano T, Mitchison T. Cell. 1994; 79:449. [PubMed: 7954811]

99. Hirano T. Nat Rev Mol Cell Biol. 2006; 7:311. [PubMed: 16633335]
100. Wood AJ, Severson AF, Meyer BJ. Nature Rev Genet. 2010; 11:391. [PubMed: 20442714]
101. Haering CH, Farcas AM, Arumugam P, Metson J, Nasmyth K. Nature. 2008; 454:297. [PubMed: 18596691]
102. Cuylen S, Metz J, Haering CH. Nat Struct Mol Biol. 2011; 18:894. [PubMed: 21765419]
103. Murayama Y, Uhlmann F. Nature. 2014; 505:367. [PubMed: 24291789]
104. Kimura K, Hirano T. Cell. 1997; 90:625. [PubMed: 9288743]
105. Kimura K, Rybenkov VV, Crisona NJ, Hirano T, Cozzarelli NR. Cell. 1999; 98:239. [PubMed: 10428035]
106. Carter SD, Sjogren C. Crit Rev Biochem Mol Biol. 2012; 47:1. [PubMed: 21923481]
107. Sun M, Nishino T, Marko JF. Nucl Acids Res. 2013; 41:6149. [PubMed: 23620281]
108. Strick T, Kawaguchi T, Hirano T. Curr Biol. 2004; 14:874. [PubMed: 15186743]
109. Cui Y, Petrushenko ZM, Rybenkov VV. Nat Struct Mol Biol. 2008; 15:411. [PubMed: 18376412]
110. Petrushenko ZM, Cui Y, She W, Rybenkov VV. EMBO J. 2010; 29:1126. [PubMed: 20075860]
111. Hirano T. Philos Trans Roy Soc Lond B. 2005; 360:507. [PubMed: 15897176]
112. des Cloizeaux J. J Phys (Paris). 1981; 42:L433.
113. Tanaka F. Prog Theor Phys. 1982; 68:148–163.Prog Theor Phys. 1982; 68:164–177.
114. Marko JF. Phys Rev E. 2009; 79:051905.
115. Baiesi M, Orlandini E, Stella AL. Phys Rev Lett. 2001; 87:070602. [PubMed: 11497876]
116. Marko JF. J Stat Phys. 2011; 142:1353. [PubMed: 21686050]
117. Jun S, Mulder B. Proc Natl Acad Sci USA. 2006; 103:12388. [PubMed: 16885211]
118. Pelletier J, Halvorsen K, Ha BY, Paparcone R, Sandler SJ, Woldringh CL, Wong WP, Jun S. Proc Natl Acad Sci USA. 2012; 109:2649.
119. Hadizadeh Yazdi N, Guet CC, Johnson RC, Marko JF. Mol Microbiol. 2012; 86:1318. [PubMed: 23078205]
120. Cui Y, Bustamante C. Proc Natl Acad Sci USA. 2000; 97:127. [PubMed: 10618382]
121. Rosa A, Everaers R. PLOS Comp Biol. 2008; 4:e1000153.
122. Marko, JF. The Mitotic Chromosome: Structure and Mechanics. In: Rippe, K., editor. Genome Organization and Function in the Cell Nucleus. Wiley-VCH; Weinheim: 2012. p. 449-486.Ch. 18
123. Uemura T, Ohkura H, Adachi Y, Morino K, Shiozaki K, Yanagida M. Cell. 1987; 50:917–25. [PubMed: 3040264]
124. Adachi Y, Luke M, Laemmli UK. Cell. 1991; 64:137–48. [PubMed: 1846085]
125. Anderson H, Roberge M. Cell Growth Diff. 1996; 7:83–90. [PubMed: 8788036]
126. Giménez-Abián JF, Clarke DJ, Devlin J, Giménez-Abían MI, De la Torre C, Johnson RT, Mullinger AM, Downes CS. Chromosoma. 2000; 109:235. [PubMed: 10968252]
127. Hirano T. Trends Biochem Sci. 1995; 20:357–361. [PubMed: 7482703]
128. Marko JF, Siggia ED. Mol Biol Cell. 1997; 8:2217–31. [PubMed: 9362064]
129. Marko JF. Chrom Res. 2008; 16:469–497. [PubMed: 18461485]
130. de Gennes, PG. Scaling Concepts in Polymer Physics. Cornell University Press: 1979. Sec. VIII. 1.2
131. Ono T, Losada A, Hirano M, Meyers MP, Neuwald AF, Hirano T. Cell. 2003; 115:109. [PubMed: 14532007]
132. Alipour E, Marko JF. Nucl Acids Res. 2012; 40:11202. [PubMed: 23074191]

Highlights

1. Review of mechanical properties of DNA and DNA-protein complexes
2. Pedagogical presentation of statistical-mechanics of DNA response to tension and twist
3. Discussion of DNA topology and topology control in cells

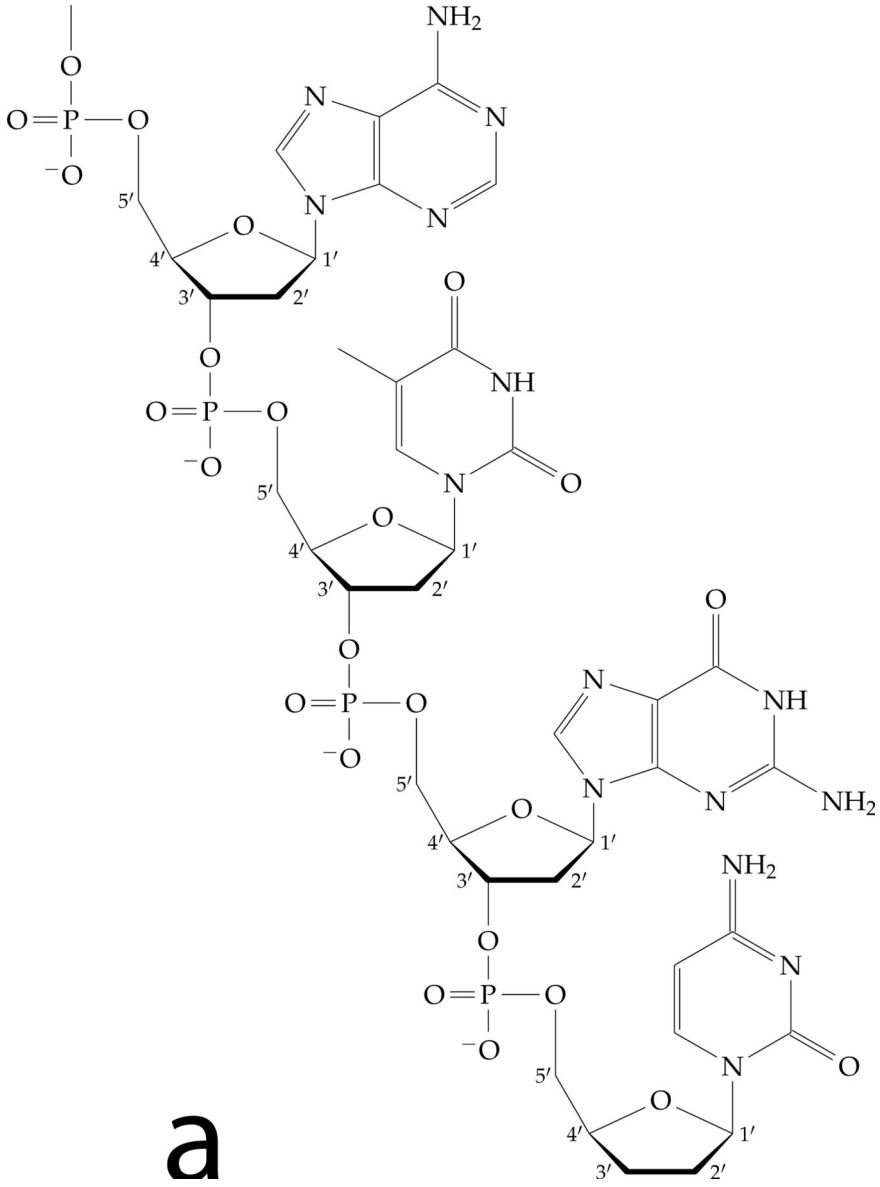

a

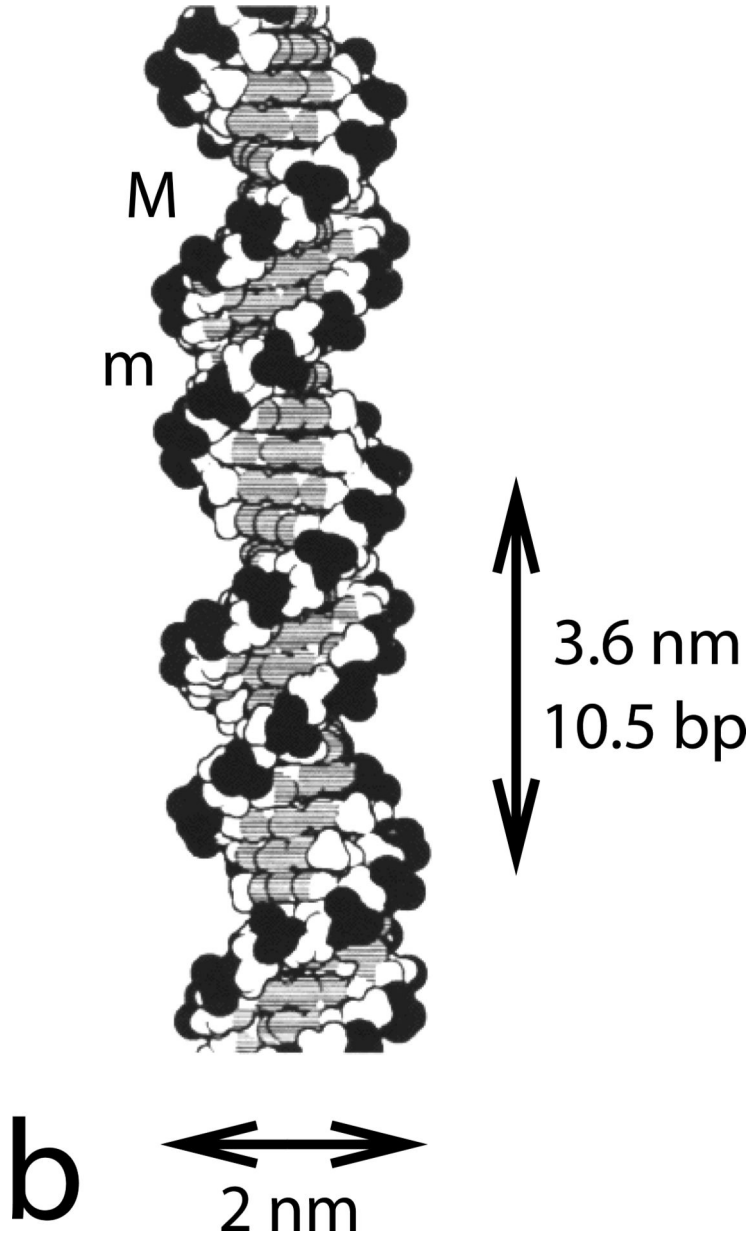

Figure 1.

DNA double helix structure.

(a) Chemical structure of one DNA chain, showing the deoxyribose sugars (note numbered carbons) and charged phosphates along the backbone, and the attached bases (A, T, G and C following the 5′ to 3′ direction from top to bottom).

(b) Space-filling diagram of the double helix. Two complementary-sequence strands as in (a) noncovalently bind together via base-pairing and stacking interactions, and coil around one another to form a regular helix. The two strands can be seen to have directed chemical structures, and are oppositely directed. Note the different sizes of the major (M) and minor (m) grooves, and the negatively charged phosphates along the backbones (dark groups). The

helix repeat is 3.6 nm, and the DNA cross-sectional diameter is 2 nm. Image reproduced from Ref. [2].

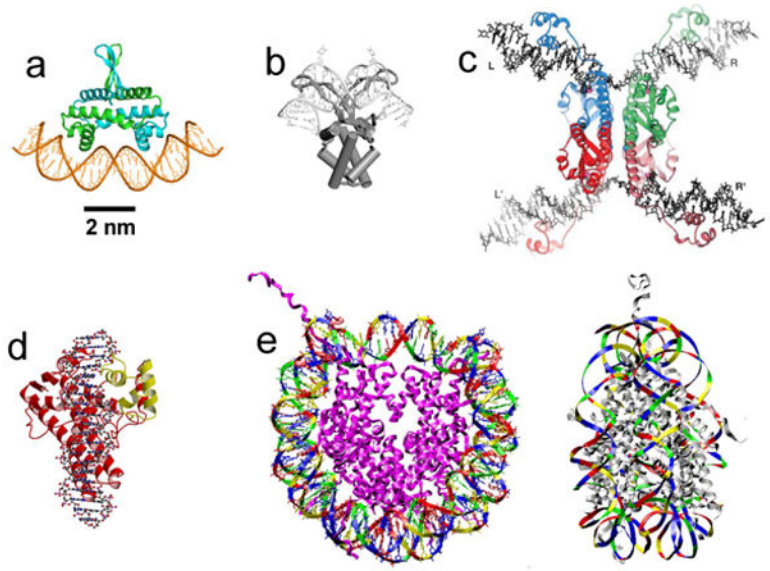

Figure 2.

Structural models of protein-DNA complexes based on x-ray crystallography studies, all shown at approximately the same scale.

(a) Fis, a DNA-bending protein from *E. coli*; the two polypeptide chains are shown in green and blue. Image courtesy of R.C. Johnson.

(b) HU, another DNA-bending protein from *E. coli*. Image reproduced from data of Ref. [3].

(c) Four resolvase proteins bound to two DNA segments. The proteins mediate cut-and-paste site-specific recombination between the halves of the DNA segments. Exchange of the cut DNAs is thought to occur by rotation of the flat protein-protein interface in the middle of the structure. Image reproduced from Ref. [4].

(d) Topoisomerase V, an archaeal enzyme that cuts one strand of DNA, allowing internal linking number of the double helix to change. Image reproduced from Ref. [5].

(e) Eukaryote nucleosome. The roughly 10-nm-diameter particle contains 147 bp of DNA are wrapped around eight histone proteins (purple chains). Top view is shown on the left, side view is shown on the right. Image reproduced from data of Ref. [6].

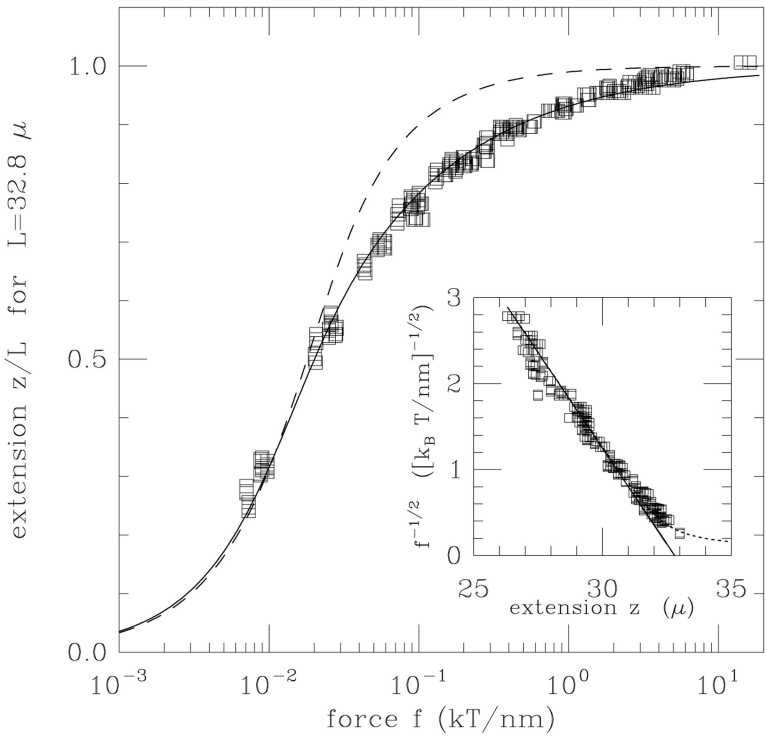

Figure 3.

Force versus extension data for 97 kb dsDNA ($L \approx 33\ \mu$m) of Smith et al [24] compared to force-extension curve of semiflexible polymer (solid curve) and freely-jointed polymer (dashed curve). Inset is proportional to $1/\sqrt{f}$ and shows a linear dependence on extension as expected for the semiflexible polymer. Note that 1 k_BT/nm = 4.1 pN. Figure adapted from Ref. [21].

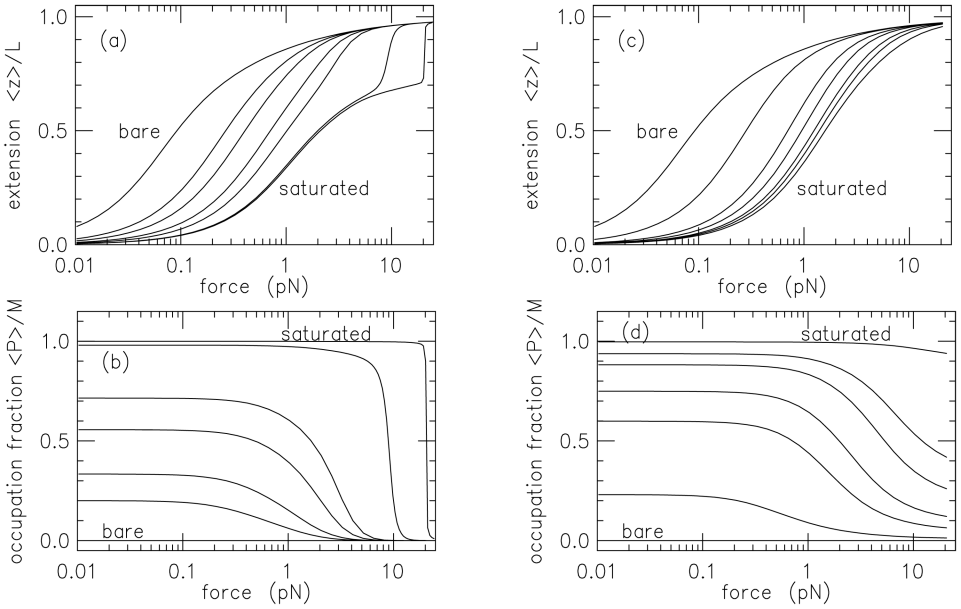

Figure 4.

Non-specificially binding DNA-bending protein; binding induces a $\psi = 90°$ bend. Segment length is $\ell = 5$ nm, and bend moduli are $a = 10$ (corresponding to bare-DNA persistence length of 50 nm). (a) Force-extension curves for stiff protein-DNA complex ($a' = 100$) for binding strengths $\mu = -\infty$ (bare DNA, leftmost curve), -2.30, -1.61, -0.69, 0, 3.00 and 6.91. The DNA straightens out and the protein unbinds at a characteristic force. (b) Protein binding site occupation corresponding to (a). the same set of binding strengths. At high binding strength the high stiffness of the DNA-protein complex causes an abrupt unbinding transition, corresponding to the abrupt extension increase seen in the corresponding curves of (a). (c) Force-extension curves for flexible protein-DNA complex ($a' = 2$) for binding strengths $\mu = -\infty$ (bare DNA, leftmost curve), -3.91, -2.30, -1.61, -0.69, 0 and 3.00. At low binding strength the force-extension curves are similar to those of (a), but at high binding strength no abrupt extension is observed due to the capacity of the DNA-protein complex to deform. (d) Protein binding site occupation corresponding to (c). Figure adapted from Ref. [55].

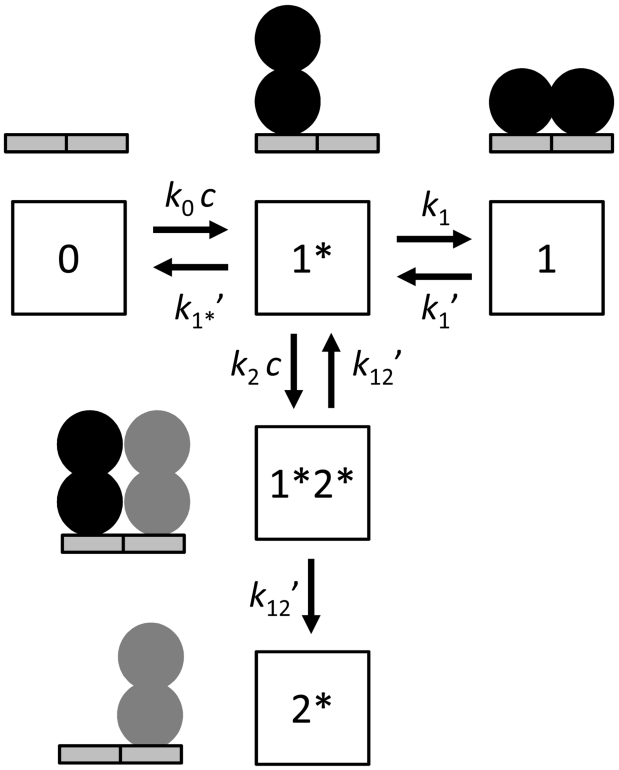

Figure 5.
Chemical reaction diagram for exchange of an initially DNA-bound protein (black balls), with a similar protein arriving from solution (gray balls), using a two bond (dimeric) mechanism.

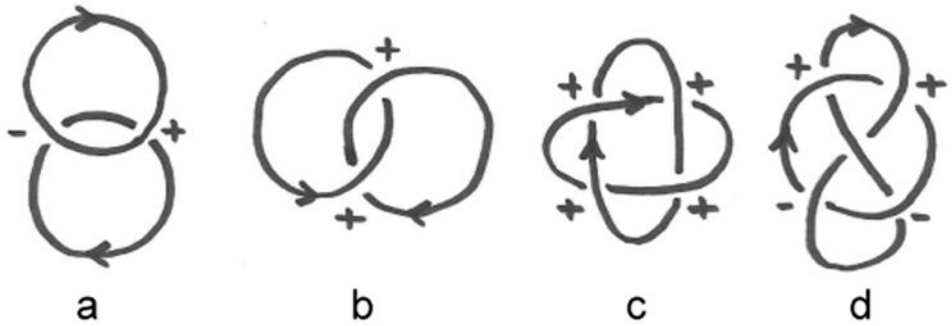

Figure 6.

Simple links of oriented loops. Lk for each pair is computed by adding up the signs of the crossings and dividing the sum by 2.

(a) unlinked rings; the signs of the crossings cancel, so Lk = 0.

(b) the Hopf link; the signs of the crossings add, so Lk = +1 (Lk would be −1 if the orientation of one of the loops were reversed).

(c) for this link (sometimes called “Solomon's knot”) the signs of the crossings again add, making Lk = +2.

(d) the Whitehead link has canceling signs of its crossings, and has Lk = 0 despite being a nontrivial link.

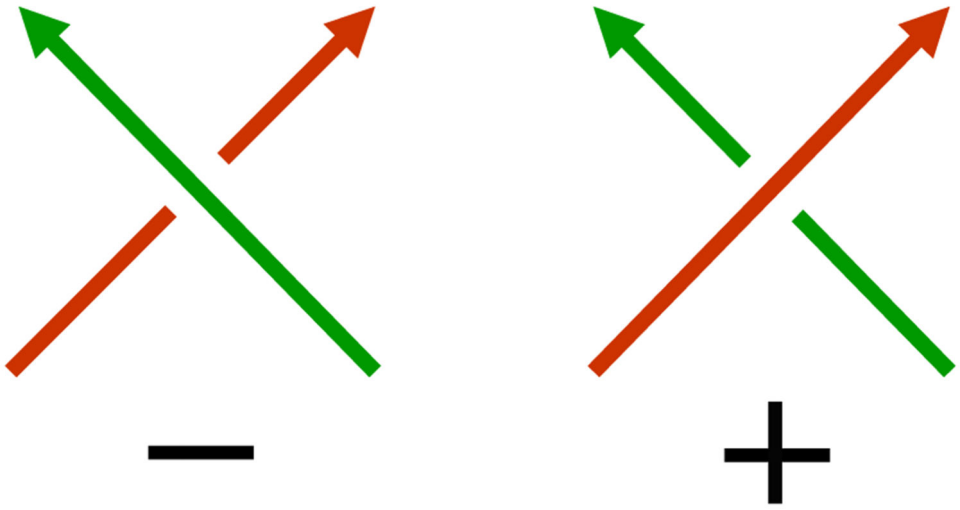

Figure 7.
Sign convention for computation of linking number using crossings. Left: left-handed (−1) crossing. Right: right-handed (+1) crossing.

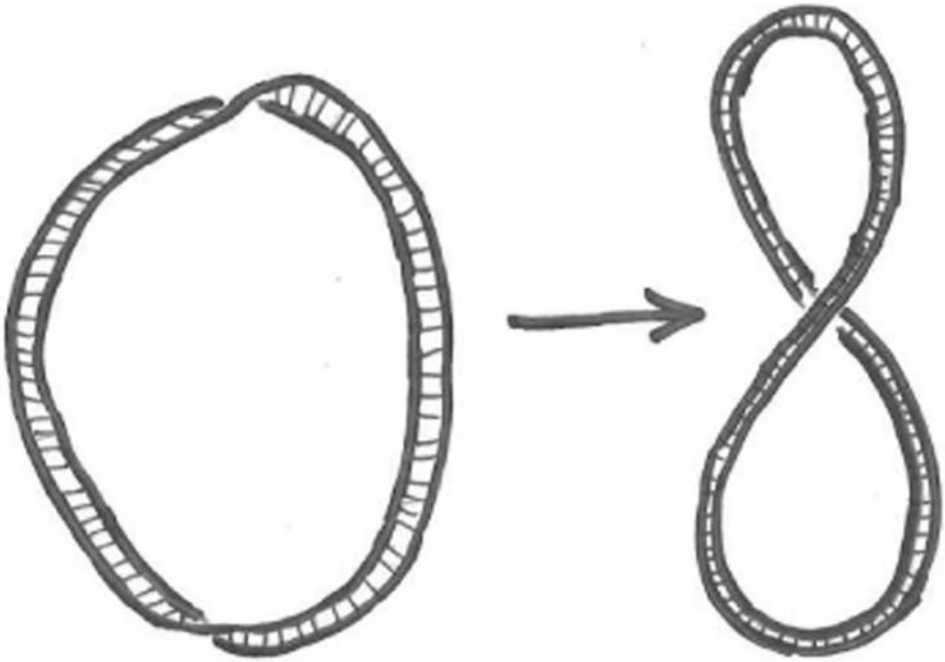

Figure 8.

Left: a ribbon with Tw ≈ −1 and Wr ≈ 0. Right: deforming the ribbon allows the twist to be transferred to writhe, so that Tw ≈ 0 and Wr ≈ −1. The linking number is fixed at Lk = −1 as long as the strip is not broken.

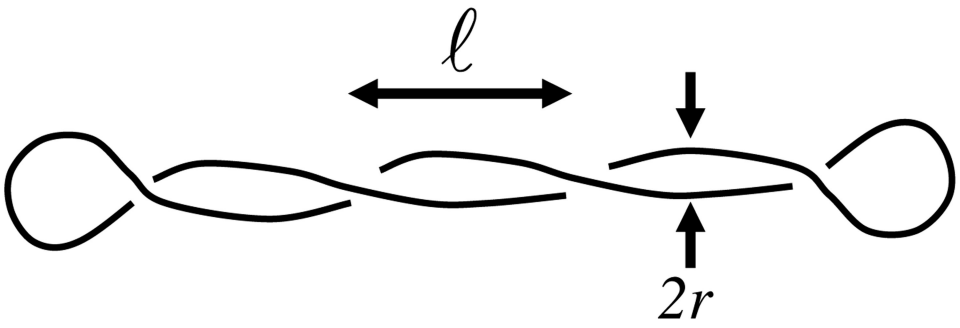

Figure 9.

Geometry of plectonemic supercoil, based on consideration of the shape as two interwound regular helices of radius r and an intercrossing distance ℓ. Note that the helix repeat is 2ℓ and the helix pitch $p = \ell/\pi$.

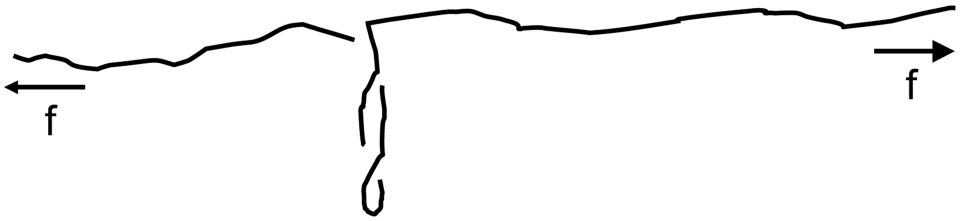

Figure 10.

Sketch of a DNA molecule under tension *f*, and with linking number fixed so as to put the double helix under torsional stress. Over a range of applied tension, the molecule breaks up into “domains” of extended and plectonemically supercoiled DNA. Only a single domain of plectonemic DNA is shown for clarity.

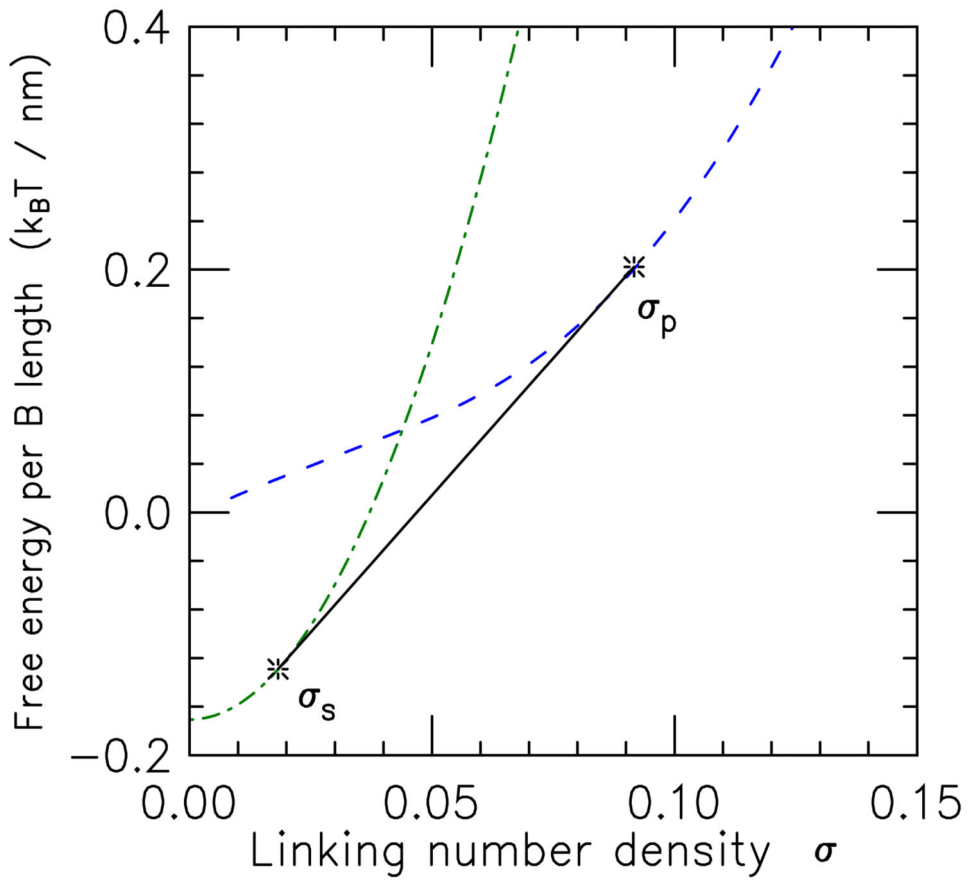

Figure 11.

Illustration of free energies of extended (dot-dashed curve, $\mathcal{S}(\sigma)$) and plectonemic supercoil (dashed curve, $\mathcal{P}(\sigma)$) DNA states as a function of linking number σ. For $\sigma < \sigma_s$, the $\mathcal{S}$ state is lower in free energy than either $\mathcal{P}$ or any mixture of the two. Similarly, for $\sigma > \sigma_p$, pure $\mathcal{P}$ is the lowest-free energy configuration. On the other hand, for σ between σ_s and σ_p the tangent construction shown (solid line segment between tangent points indicated by stars), representing coexisting domains of $\mathcal{S}(\sigma_s)$ and $\mathcal{P}(\sigma_p)$, is the lowest free energy state. Note that the gap between the two states near $\sigma = 0$ is the free energy difference between random coil DNA [$\mathcal{S}(0)$] and stretched unsupercoiled DNA [$\mathcal{P}(0)$]; this difference grows with applied force and is due to the term $-\beta f$ in the extended state free energy Eq. (39).

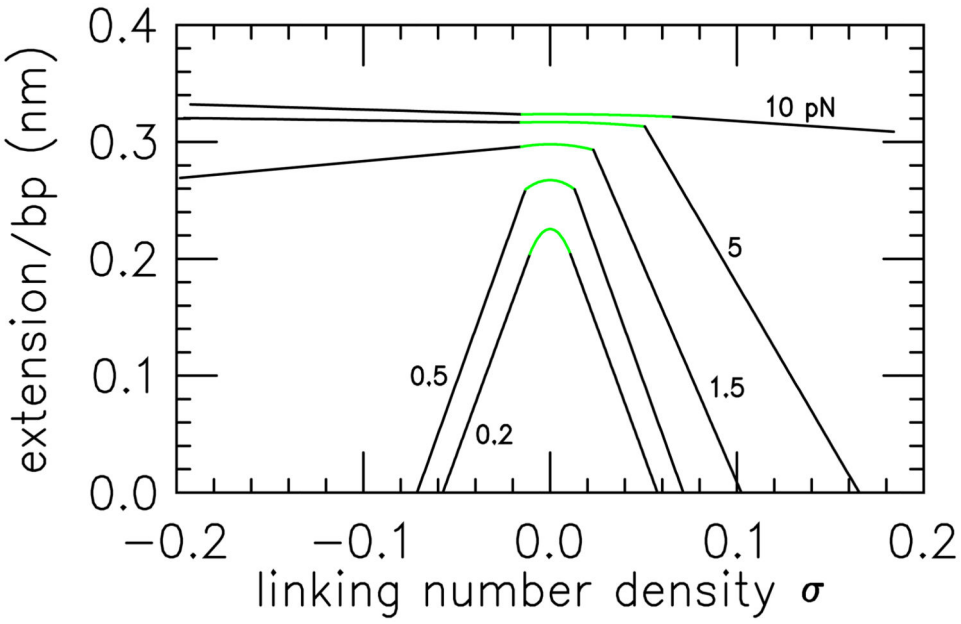

Figure 12.

Extension versus linking number curves for forces 0.2 pN (lowest curve), 0.5 pN, 1.5 pN, 5 and 10 pN (highest curve) from Ref. [82]. As force is increased, the extension increases, and the contracting effect of torsional stress (linking number) is reduced. The parabolic peak of each extension curve occurs when the DNA is purely in the extended state; extended and plectonemic DNA are in coexistence on the steep linear parts of each extension curve. The beginning of the steep black linear segments for positive supercoiling for 0.2, 0.5 and 1.5 pN, and for negative supercoiling for 0.2 and 0.5 pN indicate σ_s, and their intercepts with the σ axis indicates σ_p. For 10 pN and positive supercoiling, as well as for 2, 5 and 10 pN for negative supercoiling, formation of plectonemic DNA is pre-empted by DNA strand separation (the torque exceeds the critical torque for “melting”) with the result that a much shallower coexistence line is obtained, corresponding to coexistence of the extended state and torque-melted DNA. For details of the entire force-σ and force-torque phase diagrams see Ref. [39].

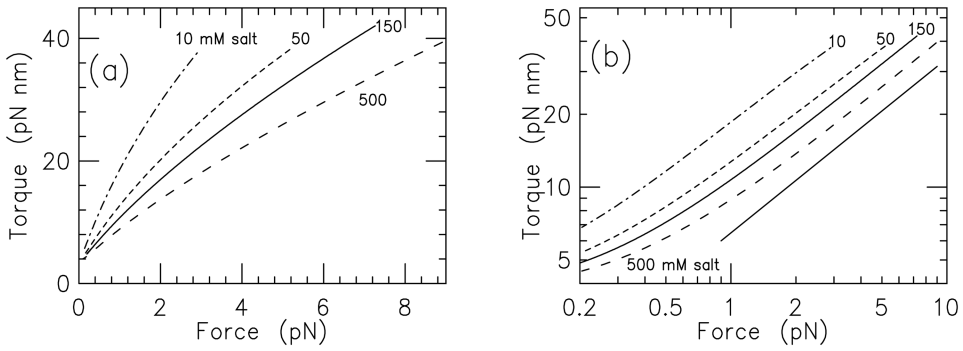

Figure 13.

Torques for extended-plectonemic supercoiled B DNA coexistence as a function of force, computed from the model of Ref. [39].

(a) As force increases, torque increases, and as univalent salt concentration is increased, the torque decreases. Results are shown for 10 mM (dot-dashed), 50 mM (short dashed), 150 mM (solid) and 500 mM (long dashed) salt.

(b) The torque follows nearly a power law in force, $\tau \approx f^{0.72}$ (solid straight line), in accord with experimental measurements [60].

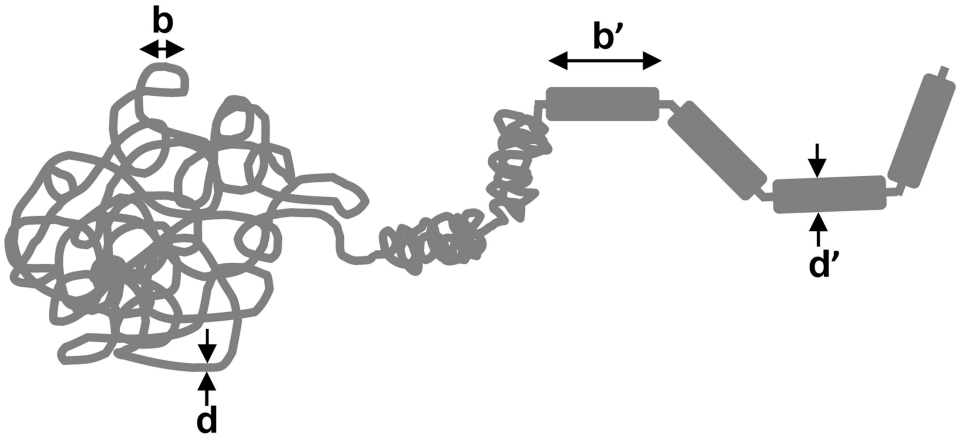

Figure 14.

Lengthwise compaction of a polymer. A segment of length *b* of thickness *d* is lengthwise-compacted into a new segment of length *b*′ and thickness *d*′. Successive segments are connected by short flexible linkers of the original polymer. As the segments become longer and thicker, entanglements are driven out of the polymer.

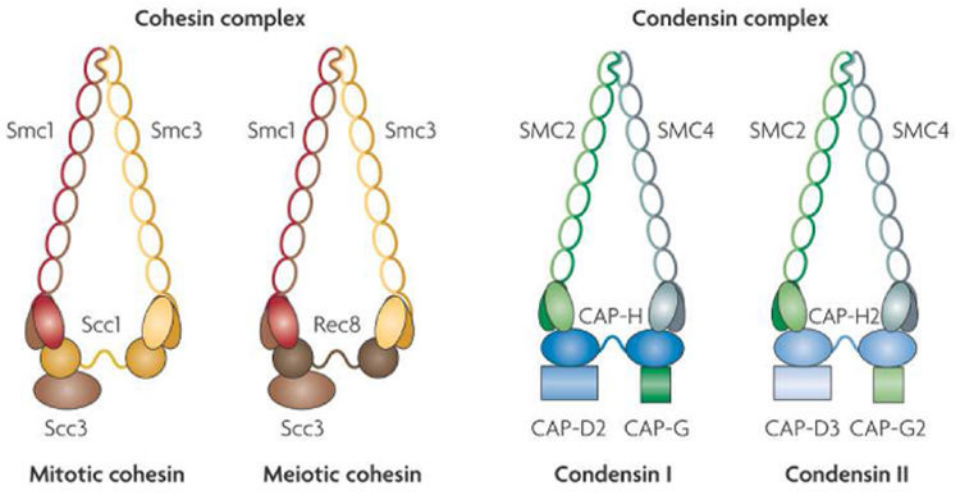

Figure 15.

Schematic diagrams of cohesin and condensin eukaryote SMC complexes. SMC complexes are built around stick-like heterodimeric SMC proteins, each of which is approximately 50 nm in length. Reproduced from Ref. [100].

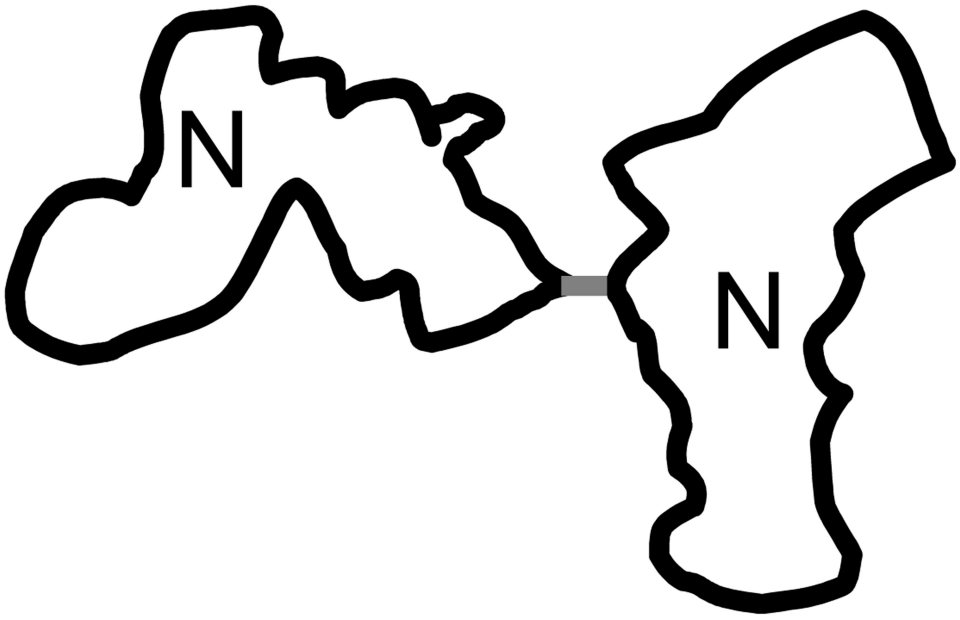

Figure 16.
Two polymers of *N* segments, joined together at one point along their contours.

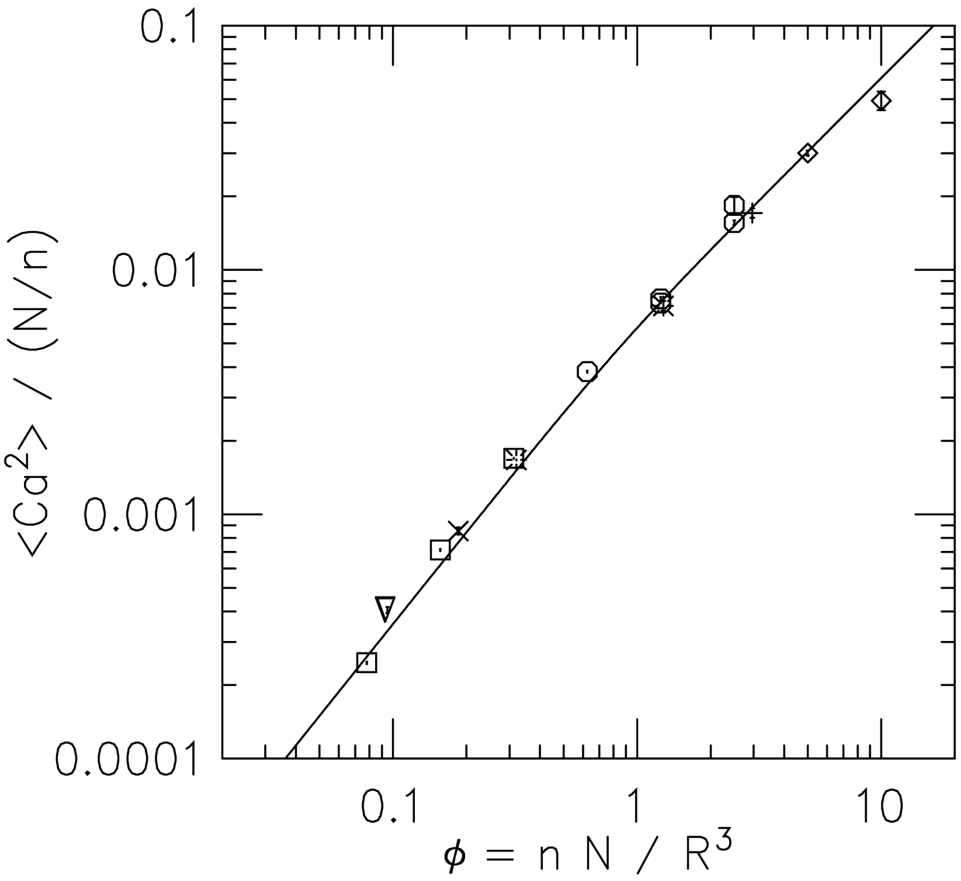

Figure 17.

Scaling behavior of catenation fluctuations for circular polymers of N unit-length segments confined to a sphere of R. The segments have a diameter 0.2 times their length ($d/b = 0.2$) and interact via excluded-volume interactions. Catenation $\langle Ca^2 \rangle / N$ scales linearly with the segment density $\varphi = nN/R^3$ for $x > 1$, and faster than linearly for $\varphi < 1$. Solid curve is a fit function that interpolates between the asymptotic behaviors $\varphi^{5/4}$ and φ^1 expected for $\varphi < 1$ and $\varphi > 1$, respectively. Figure reproduced from Ref. [116].

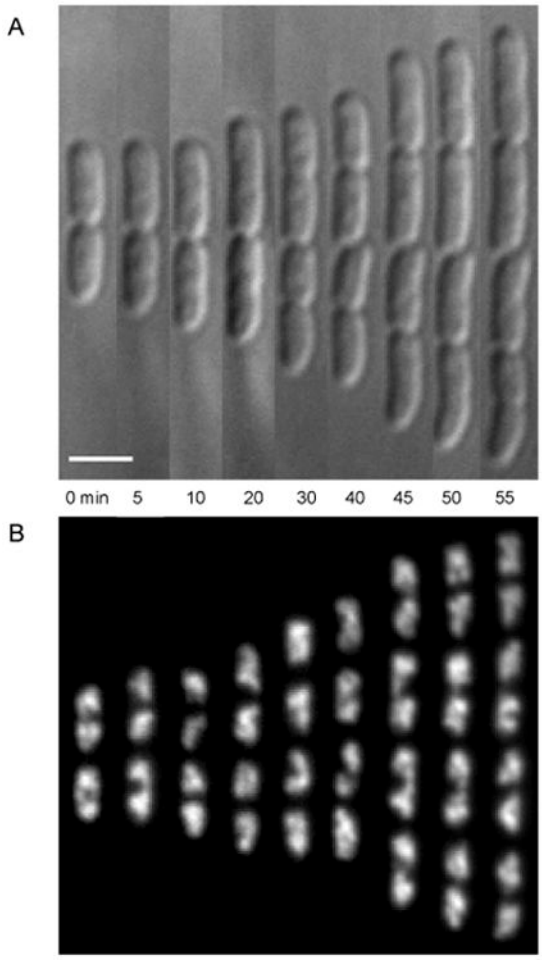

Figure 18.

Cell division (A) and chromosome segregation (B) visualized in live *E. coli* bacterial cells. The chromosomes are visualized using a fluorescent version of the chromosomal protein Fis. The chromosomes have a filamentous, coiled structure, and separate from one another well before the cells themselves divide. Bar is 2 μm. Figure adapted from Ref. [119]; see that paper for three-dimensional deconvolution analysis of the coiled chromosome shape.

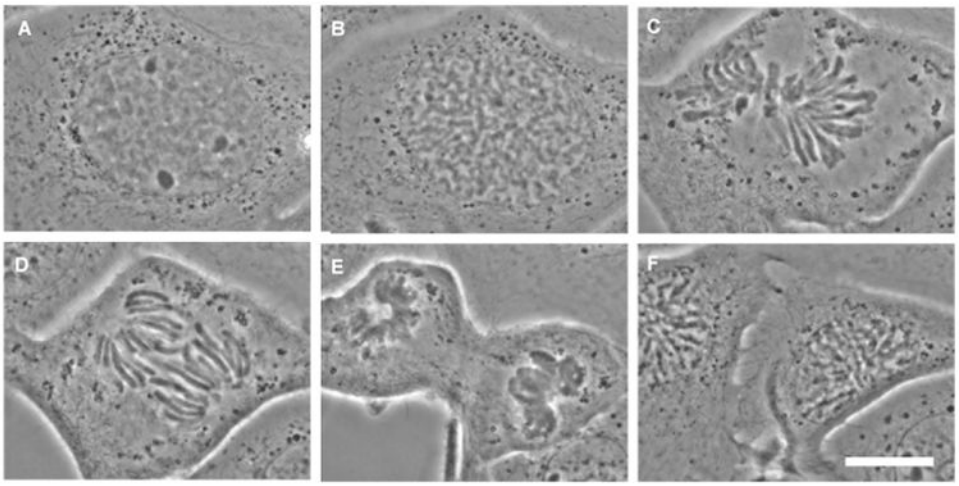

Figure 19.

Cell division (mitosis) in animal cell A: late interphase showing dark nucleoli and still uncondensed chromosomes; B: prophase showing long but condensed prophase chromosomes; C: spindle-aligned and shortened metaphase chromosomes; D: separation of chromatids at anaphase; E: telophase chromosomes beginning to decondense; F: interphase nuclei in daughter cells Bar is 20 μm Images courtesy of M.G. Poirier.